remote sensing

MDPI

Article

Evaluating Tropical Cyclone-Induced Flood and Surge Risks for Vanuatu by Assessing Location Hazard Susceptibility

Cameron Do [1,2], Yuriy Kuleshov [1,2,*], Suelynn Choy [1] and Chayn Sun [1]

1 School of Science, Royal Melbourne Institute of Technology (RMIT) University, Melbourne, VIC 3001, Australia; cameron.do@bom.gov.au (C.D.); suelynn.choy@rmit.edu.au (S.C.); chayn.sun@rmit.edu.au (C.S.)
2 Climate Risk and Early Warning Systems (CREWS), Bureau of Meteorology, Melbourne, VIC 3001, Australia
* Correspondence: yuriy.kuleshov@bom.gov.au

Abstract: Tropical cyclones (TCs) can be devastating events for vulnerable countries like Vanuatu, impacting their population, livelihoods, and infrastructure, leaving the country in need of aid and recovery. Despite this, comprehensive risk information on the nuanced impacts of each region is not well understood. Every TC event is different, and understanding the potential for impact at each location empowers decision makers in the lead-up to an event or during off-season planning to make more informed decisions to direct disaster risk reduction efforts. TC hazard model data typically describe intensity and likelihood, which can be fed into risk assessment frameworks to describe probabilistic risk. This study instead uses freely available remote sensing data to create proxies for the TC hazards of storm surge and flooding and to describe only the intensity of the hazard if the event occurs at the location. This hazard susceptibility index is fed into a risk assessment framework with Vanuatu exposure and vulnerability data for domains of populations, housing, and roads. These methods allow for the risk to be estimated for each month, as well as during specific historical time periods of TC Pam, TC Harold, and the TCs Judy and Kevin, enabling future impact validation. The results show households to have the highest risk, followed by roads and population domains, while a TC-induced surge risk is overall higher than TC-induced flooding, particularly in the road domain. The results, however, show a likely underestimation of event hazards and an overestimation of Port Vila's resistance to impacts, which is a subject of future investigation and validation.

Keywords: tropical cyclone; risk assessment; hazard; exposure; vulnerability; Vanuatu

Citation: Do, C.; Kuleshov, Y.; Choy, S.; Sun, C. Evaluating Tropical Cyclone-Induced Flood and Surge Risks for Vanuatu by Assessing Location Hazard Susceptibility. *Remote Sens.* **2024**, *16*, 1890. https://doi.org/10.3390/rs16111890

Academic Editor: Gang Zheng

Received: 3 May 2024
Revised: 21 May 2024
Accepted: 23 May 2024
Published: 24 May 2024

1. Introduction

Tropical cyclones (TCs) are powerful rotating storms that develop over warm tropical waters, with the potential to be highly destructive and costly natural disasters depending on the situation. Since 1970, more than 1900 disasters have been attributed to TCs, with almost 800,000 casualties [1], causing USD 26 billion in global damages annually [2].

While climate change is expected to reduce the frequency of TC events globally, there is an increased likelihood of major TC events with even stronger destructive power [3]. A changing climate alongside urbanisation along the coast [4] suggests the need to be wary of events in the future with an unprecedented extent and impact. An example is the formation of severe TCs outside of the usual TC season months, as was the case for TC Lola in October 2023, which became the earliest Category 5 TC on record in the Southern Hemisphere, although not directly attributed to climate change.

The potential destructiveness of TCs, their unpredictability in occurrence, as well as their rapid intensification, highlight the need for not only timely early warning systems but also risk assessment evaluations to proactively inform and prepare exposed and vulnerable communities. TCs have also been increasingly recognized as multi-hazardous, as impacts can come in the form of destructive winds as well as coastal inundation from storm surges or flooding from sustained rainfall [5–8]. Risk assessments are key tools in disaster risk reduction that collate information on the hazard, exposure, and vulnerability of the area [9]. Typically, this is in relation to human health and safety but has also been extended to infrastructure to assess the damage, as well as to see the impact on the natural environment [10–12]. They can be used by decision makers to assist the management of risk reduction funds to target the most exposed or vulnerable regions [13].

Within the literature, many TC risk studies assess TC hazards using synthetic or best-track data to model probabilistic risks [2,14–17] or assess the impacts of historical TC events [18]. While past event studies can reveal the characteristics that make a particular event impactful [19], and future probability studies can give an indication about what is more likely in the foreseeable future or inform insurance and planning, both are not designed to be used in a scenario where a TC has formed, and residents in an area of expected landfall are preparing for impact. In methods assessing future risk, the hazard considers the probability of the event occurring at a location as well as its intensity. With thousands of synthesised tracks, regions that have a higher density of tracks show higher risks of hazards. With an individual event where the track may only affect one part of the study area or which follows an unlikely but potentially impactful path, the probabilistic method assessing an ensemble of tracks can be misleading if used in a risk assessment to inform TC events as they occur. Previous methodologies have also been difficult to validate with impacts for future risk, as assessing a known TC track is fundamentally different to predicting the probability of the genesis and development of TCs in the future.

The aim of this study was to develop a methodology that can assess TC risk in a way that can inform and prepare TC-prone regions for the TC season, as well as incoming TCs when paired with track forecasts. The novel concept in this study that allows us to perform this is defining hazard as follows: 'where would receive the highest measurements if a TC event was to occur', with measurements meaning the highest storm surge or flooding as an example. By removing the probability aspect of hazard and visualising a TC event as a blanket that would affect regions equally, we shift focus onto the characteristics of the location itself and assume predicting the exact likelihood of TCs or their specific tracks to be out of scope. This information could be paired alongside the risk assessment to inform on the timescale of interest. By utilising freely accessible remote sensing data as opposed to relying on where modelled TC data are available, the method becomes much more reproducible for other vulnerable island countries in the Pacific. This hazard susceptibility method also then allows us to compare the hazard of an upcoming month against the hazard where an event occurred. In this study for Vanuatu, we investigate TC Pam, TC Harold, and the TCs Judy and Kevin combined as case study events of major TCs in our risk assessment.

With a small island developing state like Vanuatu, available modelled data were limited to global hazard models, which were coarse in their resolution, making it unsuited for a country spread out with many islands. This led to the investigation of openly available remote sensing data instead, which could characterise the propensity of different locations to hazardous events, such as storm surges and flooding. Wind hazard was not assessed as wind is almost entirely tied to the TC track and intensity, and suitable indicators to describe a location's favourability to high wind speeds were not found. The specific indicators used are explained in Section 2 on Data and Methods.

2. Data and Methods

The study area is first described in Section 2.1. Section 2.2 describes the indicators selected for the risk assessment. In Section 2.3, the method to combine indicators to calculate risk is outlined.

2.1. Study Area

Vanuatu is considered one of the most risk-prone countries in the world because of its high vulnerability, susceptibility to disasters, difficulty coping and adaptive capacity [20,21]. Vanuatu is made up of 83 islands situated in the southwest Pacific Ocean (Figure 1) and is reliant on tourism for national income and on foreign aid in the wake of natural disaster events [20,22]. Over the last 10 years, the country has been impacted by several major TCs, such as TC Pam in 2015, which caused direct economic losses of up to 60% of the country's annual GDP [23], TC Harold in 2020, and TCs Judy and Kevin in 2023. The occurrence of these TCs and many others have led to a 'boom-and-bust' cycle in the country where an influx of foreign money in the wake of disasters creates more jobs in recovery efforts, leading to a more reactionary reconstruction mindset [20] rather than trying to build long term resilience as other countries do [24]. This can also be seen through the high proportion of temporary/semi-permanent buildings. This does not mean Vanuatu should necessarily adapt to the concept of building stronger structures better for resilience, as it would not only require a high initial cost but require more maintenance for the humid, warm, and rainy conditions. Considering the intricacies of a country's situation when using risk assessments is imperative when deciding how to better prepare a country for future risk events.

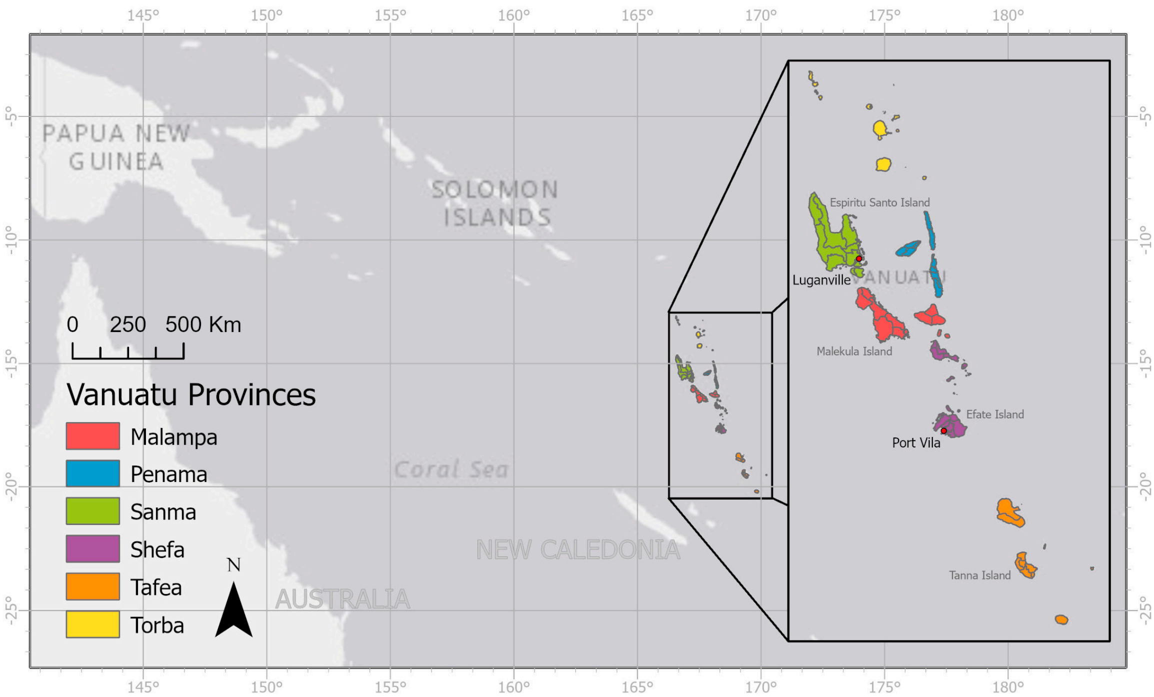

Figure 1. Map of Vanuatu in context of the South Pacific. Vanuatu Provinces are labelled, and Council Area boundaries are shown. The main cities of Port Vila (capital) and Luganville are labelled.

2.2. Selection and Description of Indicators

In this section, the selection of indicators is explained, with a focus on the hazard, as the proposed hazard index suggests an alternative way of looking at TC hazards compared to the literature.

2.2.1. Flood Hazard Indicators

The Topographical Wetness Index (TWI) was used as the first indicator for flooding, as presented by Equation (1):

$$\mathrm{TWI} = \ln\left(\frac{Specific\ Catchment\ Area}{Percent\ Slope}\right) = \ln\left(\frac{(FA+1)\times 30^2}{\left(\frac{S}{100}\right)\times 0.0001}\right) \tag{1}$$

where FA is the flow accumulation, and S is the slope. Using high-resolution Digital Elevation Model (DEM) data to derive slope and flow accumulation, it explains where water would pool based on the topographical landscape. As an example, a cell with a low TWI is less likely to be flooded and could be a feature such as the top of a hill where water runs off rather than gathers. A high TWI cell could be features such as a point along a river or a topographical depression. TWI has been used in flood hazard assessment studies before [25,26], and this study sets the basis for a methodology that uses openly available remote sensing data to explain a region's propensity to TC hazards.

The impermeability indicator was created from Land Use Land Cover (LULC) data from the European Space Agency (ESA) at a 10 m resolution based on Sentinel-1 and -2 data, which included land cover categories of grassland, forests, croplands, wetlands, mangroves, bare ground, shrubbery, built-up areas and water. In the original dataset, land use categories were assigned permeability values from 0 to 100, with 100 being the most permeable and 0 being impermeable. To create the impermeability indicator for the flood hazard index, the values were inverted by dividing by 100 and subtracting from 1. This aligned values with the logic that more impermeable land covers, such as built-up regions or water, are more prone to flooding as the surface cannot accept much water before it becomes runoff or pools on the surface. Conversely, surfaces with low impermeability, such as grasslands and forests, can receive much more water into the soil, making them less susceptible to floods. Permeability values from LULC datasets have been used in the past to inform flood hazard models but are used in this study as an independent indicator in the flood index.

The accumulated rainfall indicator is the one dynamic flood hazard indicator in this methodology. High accumulated rainfall in a short period of time leads to flooding and, for longer timescales of a month, saturates the soils, priming the conditions for flood in the future. By using Vanuatu's monthly accumulated rainfall climatology for 1980–2021 from the Multi-Source Weighted-Ensemble Precipitation (MSWEP) dataset, we differentiated the flood hazard from month to month based on the historical accumulated rainfall in each month. The MSWEP accumulated rainfall climatology by month is presented in Figure 2. Not only does this show the spatial distribution of where rainfall is most common for an island country like Vanuatu, which has islands spread over 7 degrees of latitude, but it also accounts for the dry and wet seasons by month.

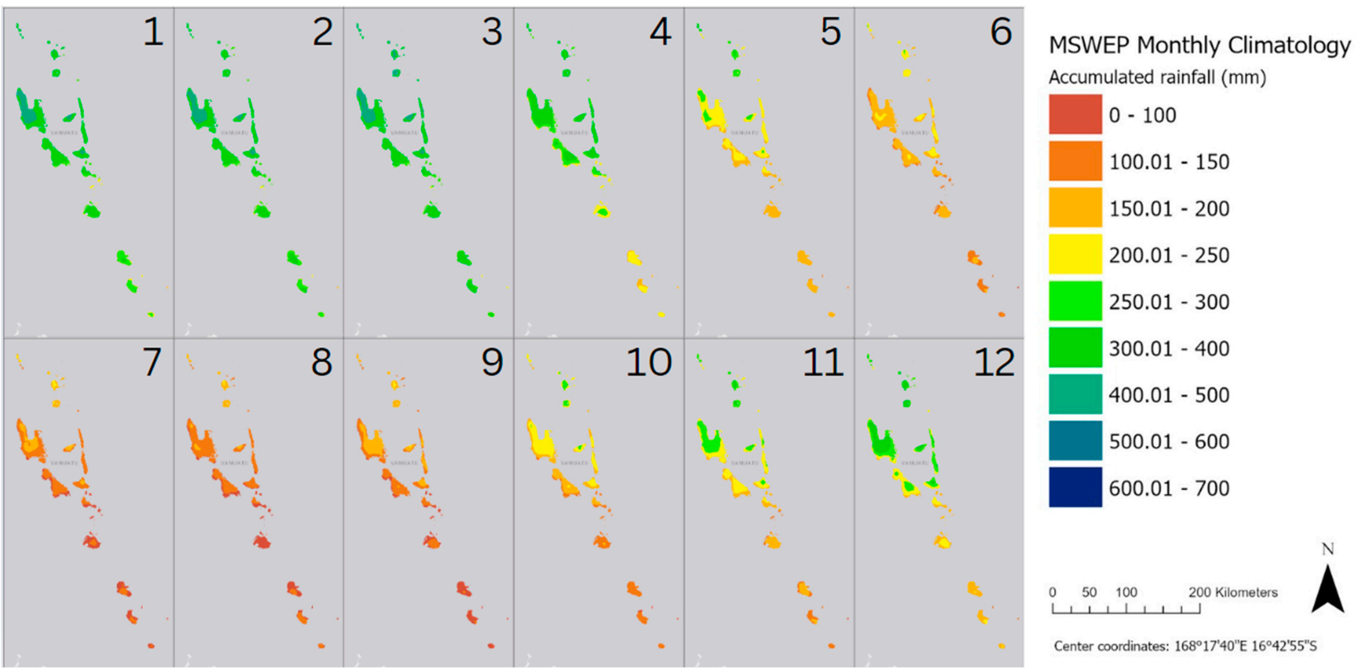

Figure 2. Accumulated rainfall averages for each month (mm) from MSWEP data for 1980–2021. Months are labelled from 1 (January) to 12 (December).

This accumulated rainfall indicator was designed not only to be dynamic from month to month based on the climatology but to also be able to receive rainfall data from historical

TC events, to calibrate and compare against expected hazards in future months, as well as to ensure the methodology could validate actual TC events and their impacts as a risk assessment. This aspect of the methodology was an adjustment to previous risk assessments, addressing the limitations of validation. To ensure that the monthly climatology accumulated rainfall and the accumulated rainfall from TC events could be compared on the same scale, we took the 5 days of highest accumulated rainfall in the TC events of TC Pam, TC Harold, and TCs Judy and Kevin, and compared them to the average or expected rainfall in 5 days of each month. The 5 days of highest rainfall were chosen by looking at daily accumulated rainfall for all days in the TCs' lifetime and summing up the 5 days that showed the highest values over Vanuatu land from a source of TC rainfall (organised convective shape). The 5-day accumulated rainfall from TCs Pam, Harold and Judy/Kevin combined are presented in Figure 3.

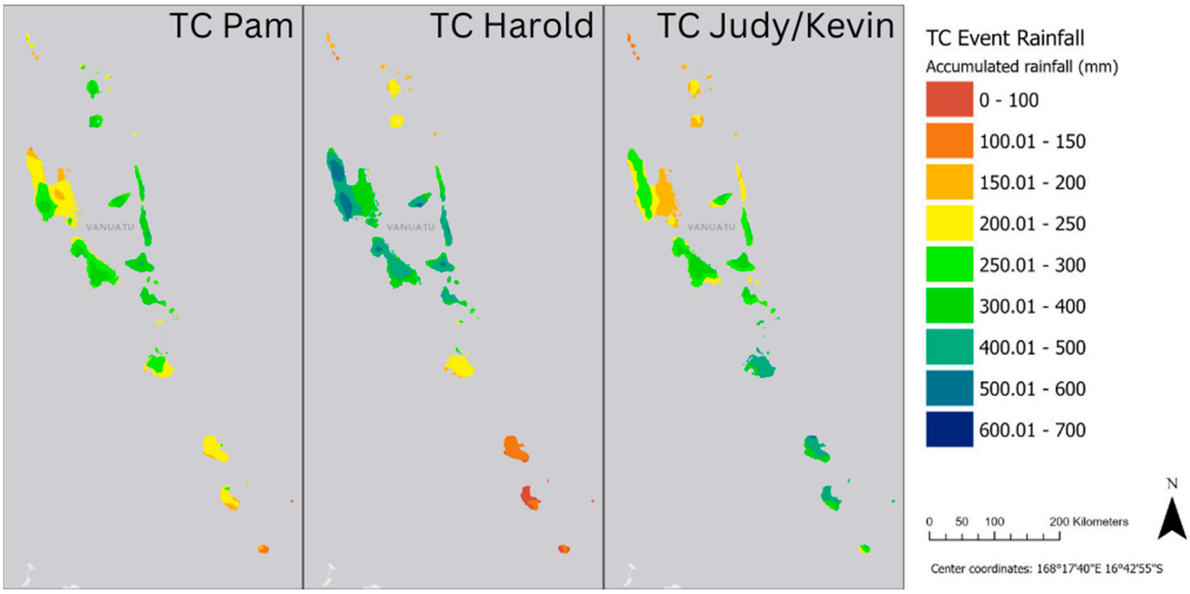

Figure 3. Accumulated rainfall (mm) over 5 consecutive days of highest TC rainfall for TC Pam, TC Harold, and TCs Judy/Kevin.

2.2.2. Storm Surge Hazard Indicators

The first indicator of the storm surge hazard is coastal elevation (CE). This indicator assessed the elevation of coastal regions and their susceptibility to inundation from the storm surge by identifying which cells would be inundated if the sea level was raised to a certain height. Scenarios of 1, 3, 5 and 7 m of increased sea levels were used in Geographical Information Systems (GIS) software (ArcGIS Pro 2.7.0) by reclassifying elevation data in each scenario to either flooded or non-flooded cells. Lower-lying coastal cells were inundated in all scenarios and, thus, were given the highest hazard values for this indicator, while regions that did not flood in any scenario were given a value of 0. This indicator identifies coastal regions across the country that are most susceptible to storm surge hazards if a TC event occurs due to their low coastal elevation.

The Shelf Gradient (SG) indicator describes how steep or shallow the underwater shelf beneath the coastline is. It is calculated as the distance from the coastline to the nearest 30 m bathymetric depth contour. This is because surge generation is mostly confined from this depth to the shore [27,28]. A coastline with a short distance to the nearest 30 m depth has a steep coastline and would be less susceptible to a storm surge compared to a coastline with a shallower gradient that allows water to reach the land more easily [28]. This was performed in GIS by isolating the 30 m depth line from GEBCO (General Bathymetric Chart of the Oceans) bathymetry data and calculating the nearest distance from each point along the coast to the 30 m depth line.

The Time Above Threshold (TAT) indicator is a dynamic indicator within the surge hazard index. TAT is defined by the time (hrs) the tide gauge measurement is above a certain high-tide threshold (e.g., 1 m) per day and attempts to describe the likelihood of an elevated tide coinciding with TC-induced storm surges. Earlier post-disaster studies have identified that the strength of a TC by its Saffir–Simpson category is not indicative of the created storm surge but that there are many other contributors, such as the size of the TC, forward speed, direction and timing [29]. Depending on whether the TC's surge coincides with high or low tide can greatly affect the total raised sea level that can inundate coasts. TAT addresses this coincidence by evaluating days with high TAT as more susceptible to surge if a TC occurs, compared to a day with only a few hours where the tide was high. To our knowledge, this concept has not been utilised within a storm surge hazard index before and is a simple way of quantifying surge propensity for each day.

TAT was created from hourly tide gauge measurement data for Port Vila from the Australian Bureau of Meteorology. As Port Vila is the only tide gauge available for Vanuatu, this study assumes similar tides and timings for the country. Hourly tide gauge data were converted into daily hours above the threshold (1 m) and then into a monthly climatology from tide gauge data in Port Vila from 1995 to 2023. A total of 1 m was chosen as a threshold to describe a raised tide, which is considerably above the baseline; however, in the future, ideally, an impact-based threshold could be investigated to align with when coastal impacts occur [30]. The average daily TAT in each month is shown in Table 1. Similarly to the flood hazard index's dynamic accumulated rainfall indicator, with our TAT dataset, we can extract the TAT values for each day of the TCs Pam, Harold and Judy/Kevin to use for comparison. TAT values from the same 5 days of the highest accumulated rainfall closely aligned with the 5 days of highest TAT values in each TC's lifetime. For each TC, the TAT values across these 5 days were averaged (Table 2).

Table 1. Average daily TAT for each month calculated from Port Vila tide gauge data from 1995 to 2023.

Month	Avg. Daily TAT (Hours)
January	10.9800
February	10.7849
March	9.95161
April	8.91071
May	8.28111
June	8.30000
July	8.80184
August	9.59447
September	9.94643
October	10.3894
November	10.5262
December	10.7454

Table 2. Average daily TAT for Port Vila tide gauge over 5 days during the TCs lifetime.

TC Event	Avg. Daily TAT (Hours)
TC Pam	12.4
TC Harold	11.6
TC Judy/Kevin	17.4

To represent future risk to TCs in this study, we selected the month of February to show in the results as it had the highest maximum accumulated rainfall and second highest TAT value out of all the months. February's hazard and risk will, therefore, be compared against that of the case study TCs in the Results and Discussion to reduce the number of figures shown; however, risk maps could be created for all months in the same way.

2.2.3. Exposure and Vulnerability Indicators

One limitation in past risk assessment studies is the lack of relevant vulnerability indicators for the non-social domain [31]. The adjustment that was, thus, made to this study to address this was first to source vulnerability data for all domains and to group exposure and vulnerability by domain. In this study, the three domains we assessed were based on each exposure indicator of population, households, and roads. Therefore, we sourced vulnerability indicators that informed how vulnerable the people, houses and roads were.

For the population domain, population density was used to inform how exposed a region was. Where there are more people per given area, the more valued assets there are at risk to TCs. To determine how vulnerable the people in each region are, the two vulnerability indicators used were Distance to Shelter (DtS) as well as an Economic Stability proxy. DtS was created within GIS by calculating the distance of each cell to the nearest communal shelter, such as schools, churches, and community centres. People living in areas that are near to a shelter are given a lower vulnerability than those with a longer distance to travel in the case where they need to evacuate their households for sturdier shelter. The Economic Stability proxy indicator was created from an income source dataset from VNSO's (Vanuatu National Statistics Office) 2016 mini-census, using the proportion of people whose main income source is from a salary. Assuming other income sources, such as fish, crop or handcraft sales, remittances or house rent, as less stable than receiving an income via salary, regions with higher proportions of main income from salaries were less vulnerable. This indicator was chosen to capture the distribution of Economic Stability across the country in the absence of more direct measures, such as total income or expendable income, which are yet to be recorded in census data.

For the housing domain, exposure was informed by Household Density. Regions with more household infrastructure had more assets to lose in the case of a TC event. The vulnerability indicators specifically related to housing were Household Wall Material and Household Roof Material. These datasets were sourced from the 2016 mini-census after the impacts of TC Pam, where VNSO gathered responses on the type of materials that were mainly used in each Council Area. For our household vulnerability indicators, from the census datasets, we took vulnerability as the proportion of households that used traditional materials for walls and palm/straw for their roofs. Households that are made up of these materials are less likely to withstand the destructive impacts of a TC if they occur compared to materials such as tile, concrete, metal, cement, or brick.

In the road domain, exposure was informed by the presence of a road at a resolution of 30 m. These data were sourced from OpenStreetMap. Compared to density indicators used for population and housing, the presence of roads is suitable for road exposure in Vanuatu, as roads are few and far between. An alternative was to create a road density indicator by counting the number of cells a road spanned across within a larger cell, but this would reduce the resolution of the indicator, making the following vulnerability indicators less appropriate. As no vulnerability data were attached to any road dataset for Vanuatu, we created a novel road vulnerability index using elevation and slope data. Guided by documentation from The Vanuatu Climate Resilient Road Standards Project [32], using GIS, we checked how many vulnerable road conditionals each road met. The conditions were as follows: intercepts a waterway, is within 50 m of the coastline, has a steep slope of >10 degrees, has a very flat slope of <1 degree, and is within 10 m of a steep slope >16 degrees. All of these conditions increase the vulnerability of roads to potential impacts of a TC. A vulnerability value of 3 was given if the road cell met 3 of the conditions, which would be more vulnerable than a road that only met one of the above conditions.

Table 3 summarises the data sources, resolution and normalisation methods used in this study for each input indicator in the risk assessment.

Table 3. Data sources, resolution and normalisation methods used for each input indicator in the risk assessment.

Indicator	Data Source	Resolution	Methods
TWI (Flood Hazard)	NASADEM-HGT elevation data	~30 m (1 arc second)	St Dev (1–7)
Impermeability (Flood Hazard)	Land Cover data from ESA	10 m	Unique (1–100)
Accumulated Rainfall (Flood Hazard)	Daily accumulated rainfall from MSWEP from 1980 to 2023	~11.1 km (0.1 degrees)	Min-max (0–1)
Coastal Elevation (Surge Hazard)	NASADEM-HGT elevation data	~30 m (1 arc second)	Unique (0–4)
Shelf Gradient (Surge Hazard)	GEBCO gridded bathymetry	~450 m (15 arc seconds)	Quantile (1–10)
TAT (Surge Hazard)	Hourly Sea Level and Meteorological Data from the Australia Bureau of Meteorology from 1995 to 2023	N/A	Min-max (0–1)
Population Density (Population Exposure)	Vanuatu Population Density 2020 (WorldPop)	1 km	Quantile (1–10)
Distance to Shelter (Population Vulnerability)	Vanuatu Buildings polygons (OpenStreetMap)	30 m	Quantile (1–10)
Economic Stability (Population Vulnerability)	Proportion of households with salary as main income (Vanuatu 2016 mini-census)	Council Area level	Equal (1–9)
Household Density (Housing Exposure)	Household locations grid (2016 Population and Housing census)	100 m	Quantile (1–10)
Household Wall Material (Housing Vulnerability)	Proportion of houses built with traditional materials for walls (Vanuatu 2016 mini-census)	Council Area level	Equal (1–10)
Household Roof Material (Housing Vulnerability)	Proportion of houses built with palm/straw materials for roofs (Vanuatu 2016 mini-census)	Council Area level	Equal (1–10)
Road presence (Road Exposure)	Vanuatu Road polylines (OpenStreetMap)	30 m	Unique (1)
Road Vulnerability Index (Road Vulnerability)	NASADEM-HGT elevation data	~30 m (1 arc-second)	Unique (0–4)

2.3. *Outline of Method*

While this study focuses on the use of remote sensing data as proxy hazard indicators, how a hazard is combined with exposure and vulnerability follows the same risk assessment framework as previous studies [31]. Major improvements from the authors' previous study include calculating data at a gridded high resolution, separating exposed domains to assess their relevant vulnerability, and assessing risk for different time periods based on dynamic hazard indicators. Indicator data were sought for categories of hazard (flood and storm surge), exposure (population, housing and road domains), and vulnerability (population, housing and road domains).

Classification methods were carefully chosen based on each indicator and the shape of their dataset. Defined equal intervals were used for data related to the % proportion per Council Area from census data, whereas the quantile was used for indicators like population and household densities. A min–max linear normalisation was used for the dynamic hazard indicators of accumulated rainfall and TAT to allow case study TC events to contextualise monthly values, setting the max range. Unique values of integers 0–4 were used for indicators based on scenarios such as coastal elevation and the road vulnerability index. Once classified, all indicators were normalised to a 0–1 value before being placed into index and risk calculations.

The risk calculation we used in this study follows what is commonly used in the literature, where risk is the product of hazard, exposure and vulnerability [33,34], as presented by Equation (2). For a region to be at risk, there must be exposed assets with some vulnerability to the potential hazard.

$$Risk = Hazard \times Exposure \times Vulnerability \tag{2}$$

The hazard index value, which is used in the risk equation, was calculated by equally weighting and averaging each hazard indicator. This was conducted separately for the two hazards of flooding and storm surge. In the case of multiple vulnerability indicators, such as for population and housing domains, they were also averaged and then multiplied by their relevant exposure indicator. Each hazard was then multiplied by each domain's exposure vulnerability product. A visual representation is given in Figure 4. This resulted in maps at a 10 m resolution for all of Vanuatu for risk to populations, housing and roads, and for both TC-induced flood and storm surge. Additionally, risk maps were created for case study events of TCs Pam, Harold and Judy/Kevin by replacing monthly accumulated rainfall and TAT values for the values measured at the time of each event.

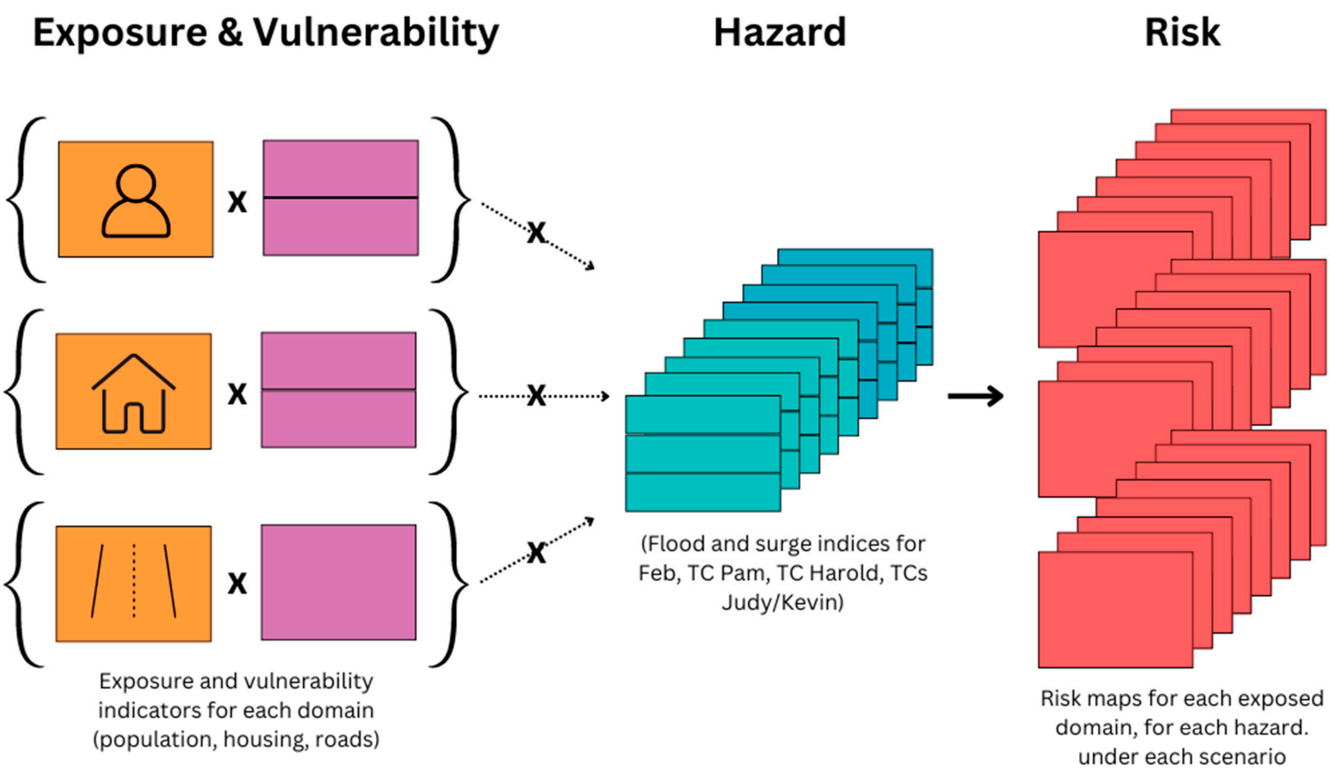

Figure 4. Visual representation of the risk calculation process from domain-specific exposure and vulnerability indicators, flood and surge indices for different time periods, and the resultant risk maps produced.

3. Results and Discussion

In the following sections, maps of indicators to the final risk map results are shown and described before trends and insights are discussed. The flood hazard is discussed in Section 3.1, followed by the surge hazard in Section 3.2. Exposure and vulnerability of the three assessed domains are discussed in Section 3.3, followed by risk in Section 3.4. Further discussion can be found in Section 3.5. In some cases, the results are shown for the specific area of greater Port Vila to capture high-resolution trends; however, results have been computed for all of Vanuatu.

3.1. Flood Hazard

The reclassified Topographical Wetness Index (TWI) values mapped over Port Vila and southern Efate Island are presented in Figure 5.

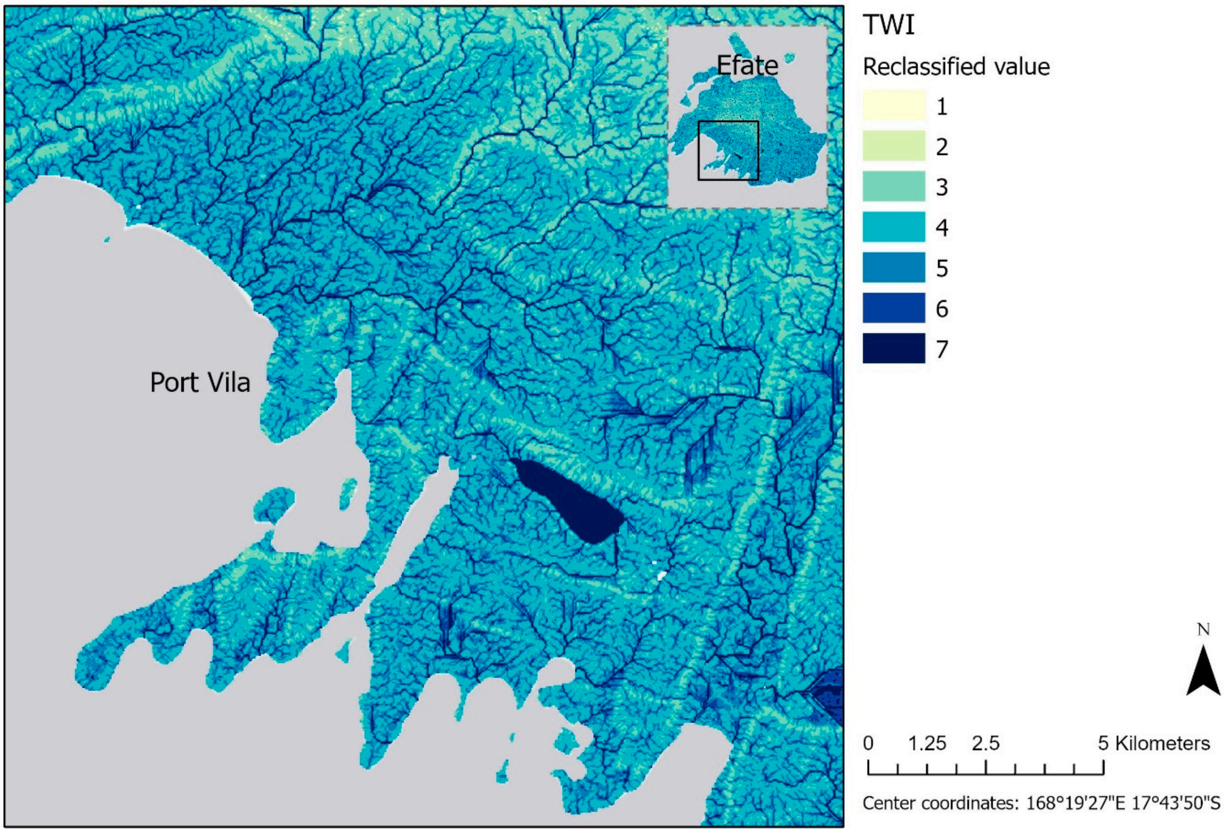

Figure 5. Reclassified Topographical Wetness Index (TWI) values mapped over Port Vila and southern Efate Island.

Figure 5 shows darker blue areas to have a higher reclassified value for TWI as an indicator of the flood hazard. Topographically, flood-susceptible areas are those of lower elevations than their surroundings, and TWI captures this by considering the elevation and slope. TWI also describes where water can flow and pool to first in a flood event when considering flow accumulation in its equation. In Figure 5, many river patterns can be seen, including areas that could act as rivers with enough water. Additionally, lighter colour ridges can be seen, especially towards the centre of Efate and its mountains. The dark blue lake-like feature with the highest TWI values is actually Emten Lagoon, which is an example of where water could pool in. TWI is combined with the other flood hazard indicators; however, Emten Lagoon is masked out as part of the ocean. Over the main city of Port Vila, TWI values are generally lower without the presence of such dark rivers running through it.

TWI is an ideal indicator for the TC flood hazard as it only requires high-resolution DEM data, which are readily available globally, and creates an indicator that shows differences in flood susceptibility in great detail.

The impermeability indicator of the TC flood hazard is shown in Figure 6.

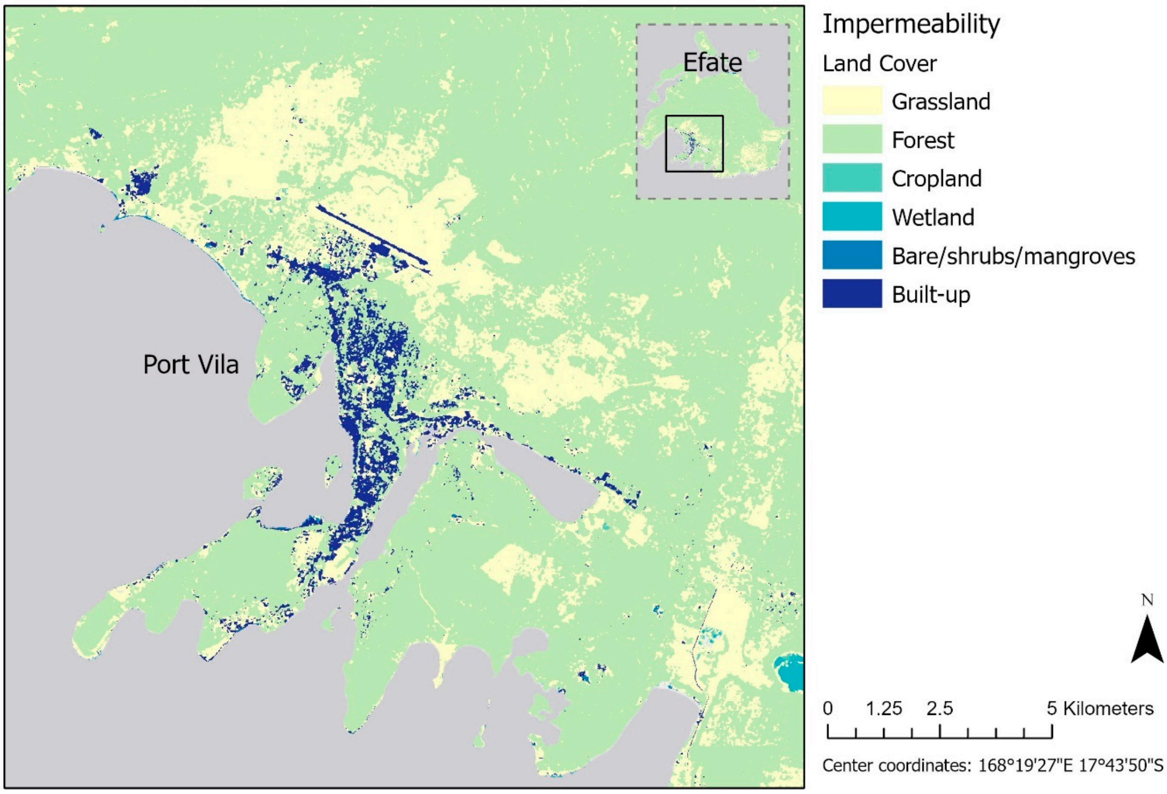

Figure 6. Impermeability classed by land cover type mapped over Port Vila and southern Efate Island.

Darker land cover refers to areas that are more impermeable and, thus, are more susceptible to flooding. Built-up urbanised land cover had a value of 80, while bare ground, shrubs and mangroves had a value of 65; wetlands were 60, cropland was 45, forest was 30, and grasslands were the least impermeable with a value of 15. In index calculations, these impermeability values were divided by 100 for a value from 0 to 1. For Vanuatu's capital of Port Vila on Efate Island, the highest impermeability was seen across the city with built-up land cover. At the northern end of Port Vila is the airport, which can be seen as a long line of dark blue. This makes sense as built-up areas generally have more paved surfaces, which take in less amounts of water before turning excess water into runoff that can begin to pool. Apart from the city, Efate and most other islands in Vanuatu are dominated by forest land cover and some grasslands, which have some of the lowest impermeability values and contribute to lower flood hazards.

Similarly to DEM data, the land cover data used in this study are freely available globally, making it feasible to apply this methodology to other TC- and flood-prone countries. At an even higher resolution (10 m) than DEM, impermeability is another physical indicator that provides great detail to the flood hazard index.

The AR indicator for the month of February directed towards future risk for the month, as well as the historical case study events of TC Pam in 2015, TC Harold in 2020, and TCs Judy and Kevin in 2023, are shown in Figure 7.

For February, values are low across the country, with slightly higher values of 0.1–0.2 across parts of the northern islands (Figure 7a). For TC Pam, AR is highest in the northeast in the Penama province with a max of 0.6–0.8, with moderate values across the rest of the country despite being far from the TC track (Figure 7b). For TC Harold, maximum AR values are reached in Sanma province and parts of Penama province within 100 km of the TC track. Port Vila received moderate rainfall, while more southern islands received values of 0–0.2 (Figure 7c). For the TCs Judy and Kevin, AR was highest in Shefa and Tafea provinces, where the two TC tracks both passed through, with moderate values along the northern path of TC Judy and west of Luganville (Figure 7d).

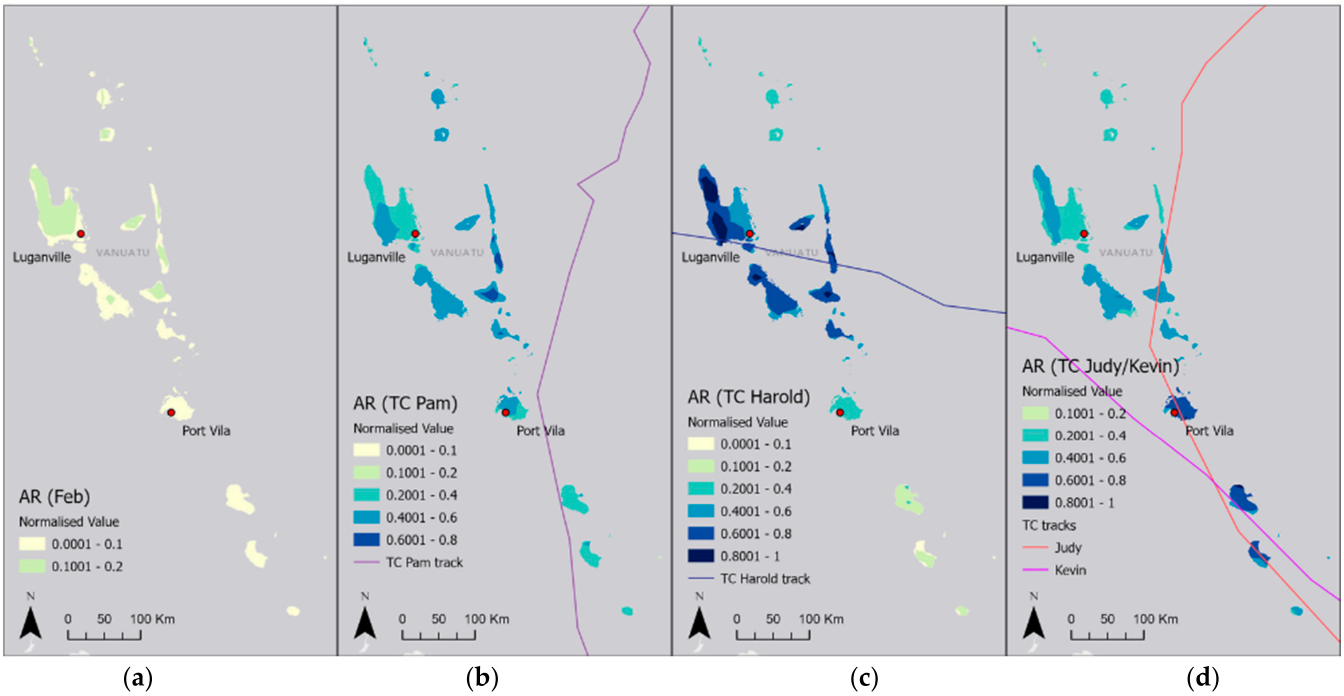

Figure 7. Accumulated rainfall (AR) values normalised by highest raw value from TC Harold, across Vanuatu for the month of February (**a**), and TC case study events for the TCs Pam (**b**), Harold (**c**), and Judy/Kevin (**d**).

The regions of higher (0.1–0.2) AR values in the February map show which regions have received more rainfall on average in the month of February since 1980. These light green regions seem to correlate with higher elevation and mountainous features in the northern islands. Despite there also being mountains in Efate and more southern islands, rainfall seems to be more common in the north, closer to the equator. Values for February were very low compared to those from the case study TCs. This is because the expected AR over 5 days in February is compared to 5 days during a rare extreme TC event. Within the method, the maximum accumulated rainfall value over 5 days found for TC Harold was used as the maximum value in the linear normalisation of all maps. This set the highest value of one as the amount of rainfall reached the wettest spot during TC Harold, giving meaning and perspective to all other values. In previous risk assessments, indicator values often were not calibrated to anything meaningful [31], limiting observations to just comparative statements, such as one region had higher values than another and thus would contribute to higher risk.

For the three case study TCs, it can be seen that the highest AR does not necessarily follow the TC track, particularly for TC Pam. TC systems can be quite large, and most rainfall does not necessarily fall near the centre; rather, how long a system resides over an area can contribute more to accumulated rainfall. This is supported by the two tracks of TCs Judy and Kevin passing over the same southern islands of Vanuatu, as well as the high AR in TC Harold, where the TC spent a lot of time west of Vanuatu outside of the map frame before gradually moving east over the country.

When comparing the month of February to the TC case study events, the very high hazard values in an event that occurred contribute to much higher risks in the risk assessment below. This is to be expected as these three events did cause massive damage and negatively impacted the country's population, infrastructure and livelihoods. For the future risk map, where we used February's average rainfall values, we identified regions that generally received more rainfall in the month due to spatial location and topographical features. This may contribute to wetter antecedent conditions and is used to estimate regions of highest risk in the future when TCs have yet to form, and tracks cannot be predicted.

By combining the three flood hazard indicators TWI, impermeability, and AR, the flood hazard index is created, as shown in Figure 8.

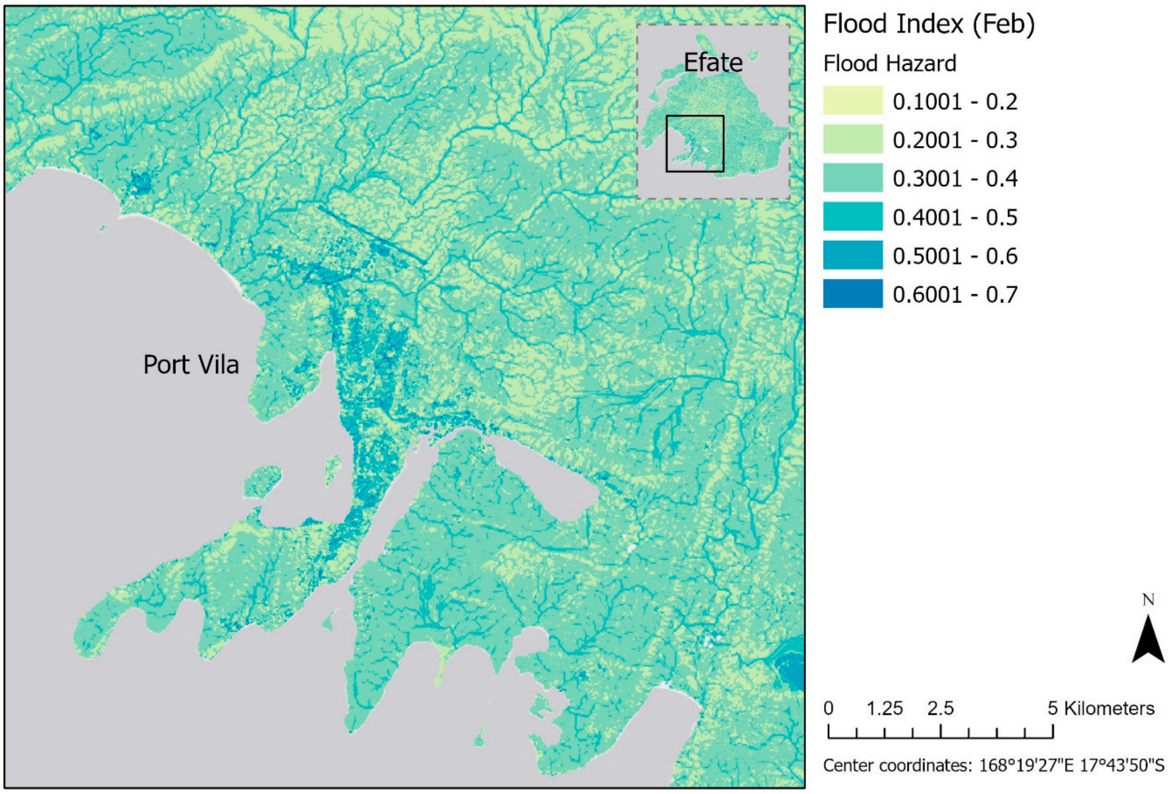

Figure 8. Flood hazard index values for February shown over southern Efate Island.

The flood index for February in Figure 8 shows similar patterns identified in the TWI and impermeability indicators, with higher values where these patterns overlapped. In particular, urban Port Vila has higher values, along with the airport strip north of the city. Outside of Port Vila, the river systems and ridges from the TWI indicator can be seen. The influence of the AR indicator is indiscernible as rainfall data came at a lower resolution and had little variation over small distances.

For the three TC case study events, we expected similar patterns to be identified in Figure 8 at a high resolution but with amplified values for regions with higher event rainfall.

3.2. Surge Hazard

Coastal elevation (CE) over Port Vila and its surroundings is shown in Figure 9.

Regions with higher CE values are areas that become inundated with 1 m of storm surge with higher thresholds for lower values. CE is shown to be high, particularly on the west coast of Port Vila and at several parts along the southern coast. Of note is Emten Lagoon, which, as explained earlier, is masked out as part of the ocean in index calculations. Another consideration is that CE did not simulate how water could reach further inland but was only based on elevation in situations of elevated sea levels to emulate surges. As a result, some inland regions, particularly in the southeastern map extent, have >1 values far inland, separated from the ocean by higher elevation barriers.

The CE indicator shows low-lying coastal regions that are most susceptible to the storm surge hazard. By mapping where these regions are, we overlay with other surge indicators to determine where we estimate surges to be the highest in a TC event; understanding this, in reality, depends on the strength, extent and direction of the particular TC. One of the limitations noted above is how far inland areas can still show >1 CE values despite not being connected to the coast by a lower elevation channel. This is not addressed as the method intersects this indicator with the Shelf Gradient indicator, which only has values up to 200 m from the coast. Another point to note is that Vanuatu is one of the Pacific Island countries that is uplifting due to tectonic processes [35], which helps to reduce the impacts of rising sea levels with climate change. This does not negate the need for storm surge risk assessment, however, as some high-hazard areas have been identified, and most of Vanuatu's populations and infrastructure are lined around the coast and rely on fishing activities.

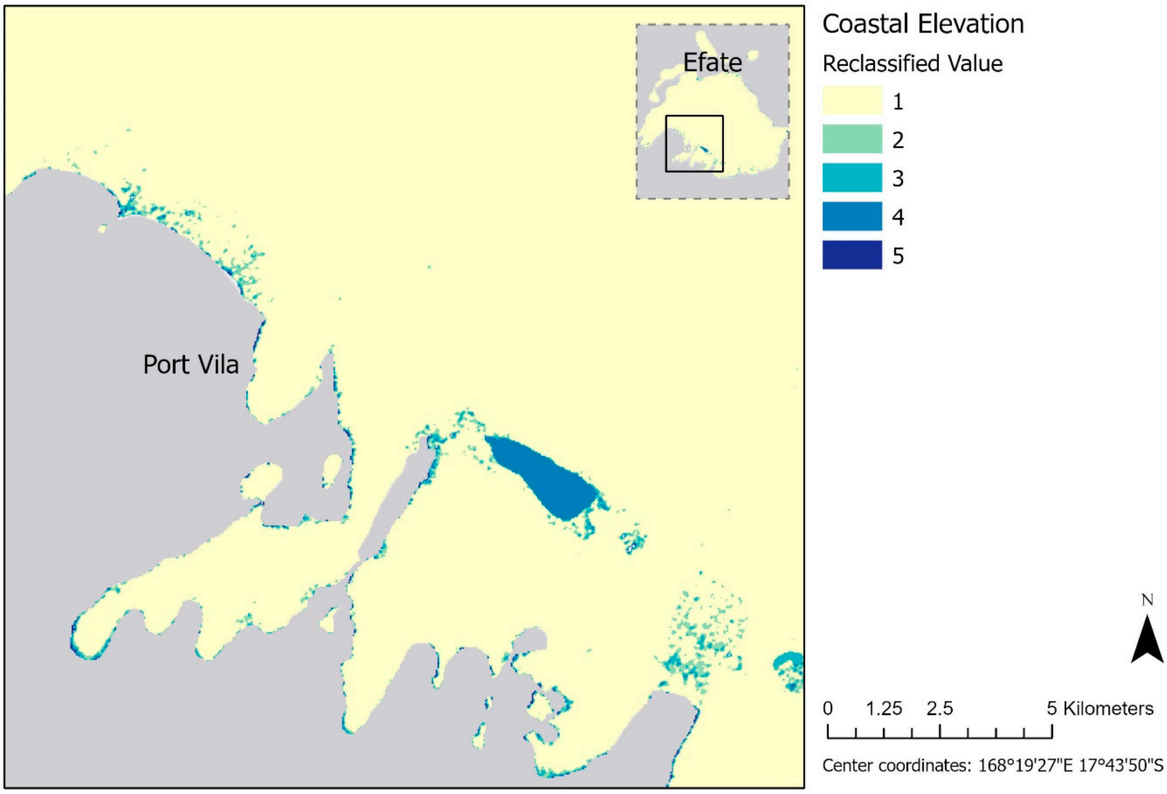

Figure 9. Reclassified coastal elevation values over southern Efate Island, describing low-lying regions susceptible to inundation.

The Shelf Gradient (SG) indicator is shown within 200 m of the coastline of Port Vila and its surroundings in Figure 10.

The further away from the dotted green line describing 30 m bathymetric depth, the shallower the gradient underwater is for storm surges to run up. A shallower, hence, further away coastline is given a higher reclassified hazard value versus a steep gradient, which is given a lower value. High values around Port Vila are seen around the lagoons and along the southern coastline, where the coastline curves inland like a bay. Lower values are seen in western Port Vila and around the southwestern peninsula. It can be noted that sometimes the 30 m bathymetric depth line crosses into land due to the inaccuracies of the lower resolution bathymetry data.

A 200 m buffer from the coastline was used to limit the surge risk assessment to land within 200 m of the coast. This was seen as a generous length to capture surge impacts and capture most regions with moderate-to-high values in the coastal elevation indicator. One concern with the indicator, however, is its usability as an indicator for coastlines that reach far inland, such as lagoons. The purpose of this indicator was to distinguish steep open coastlines against bay-like coastlines, which allow the shallow run-up of storm surges more easily [28]; however, for Vanuatu with a more complex coastline shape, as shown along the south of the extent in Figure 10, the suitability of the indicator to Vanuatu should be assessed in future validation.

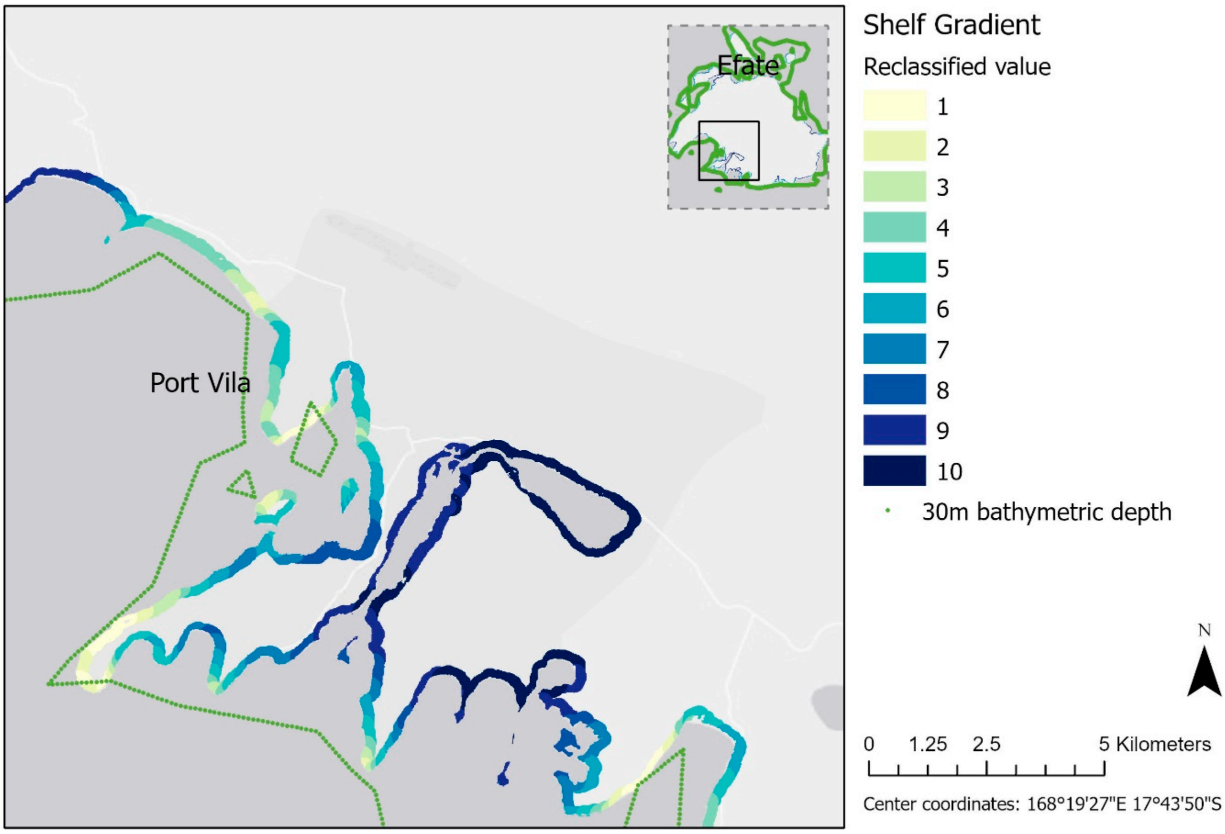

Figure 10. Reclassified Shelf Gradient values along the coastline of southern Efate Island. The dotted line of 30 m bathymetric depth is shown.

The recorded tide gauge sea level and calculated Time Above Threshold (TAT) are plotted for the three TC case study events in Figure 11.

TAT describes the amount of time per day the tide was above a threshold of 1 m and was chosen to indicate the likelihood of a raised tide level coinciding with a TC event's storm surge for each day. Figure 11 above shows both the sea level values (a, c, e) and TAT (b, d, f) from three days before to three days after the case study TC events. The averaged TAT value from 5 days of each TC event is normalised and used as a flat value across the country as the TAT indicator value. After normalisation, these values were 0.45 for TC Pam, 0.36 for TC Harold, and 1.0 for TC Judy/Kevin. In comparison, the average value for the month of February was 0.27.

Investigating the trend of TAT before, during, and after each TC event in Figure 11, one can see that TAT rises during an event and often decreases below pre-event levels once the TC has passed. Of consideration is that these TCs could not have caused landfall in Port Vila or had their strongest storm surge at the same point in the 5 days of the TC's effective lifetime that we investigated. Comparing event-averaged and normalised TAT values for each TC in their preceding daily TAT values, we can see that high preceding daily TAT values correlate with high-event TAT values, and thus reinforce the use of this indicator to show monthly/seasonal TAT value variations and how they can contribute to an increased TC surge risk. With more tide gauge locations, similar values could be derived for each location to better spatially assess storm surge hazards based on TAT.

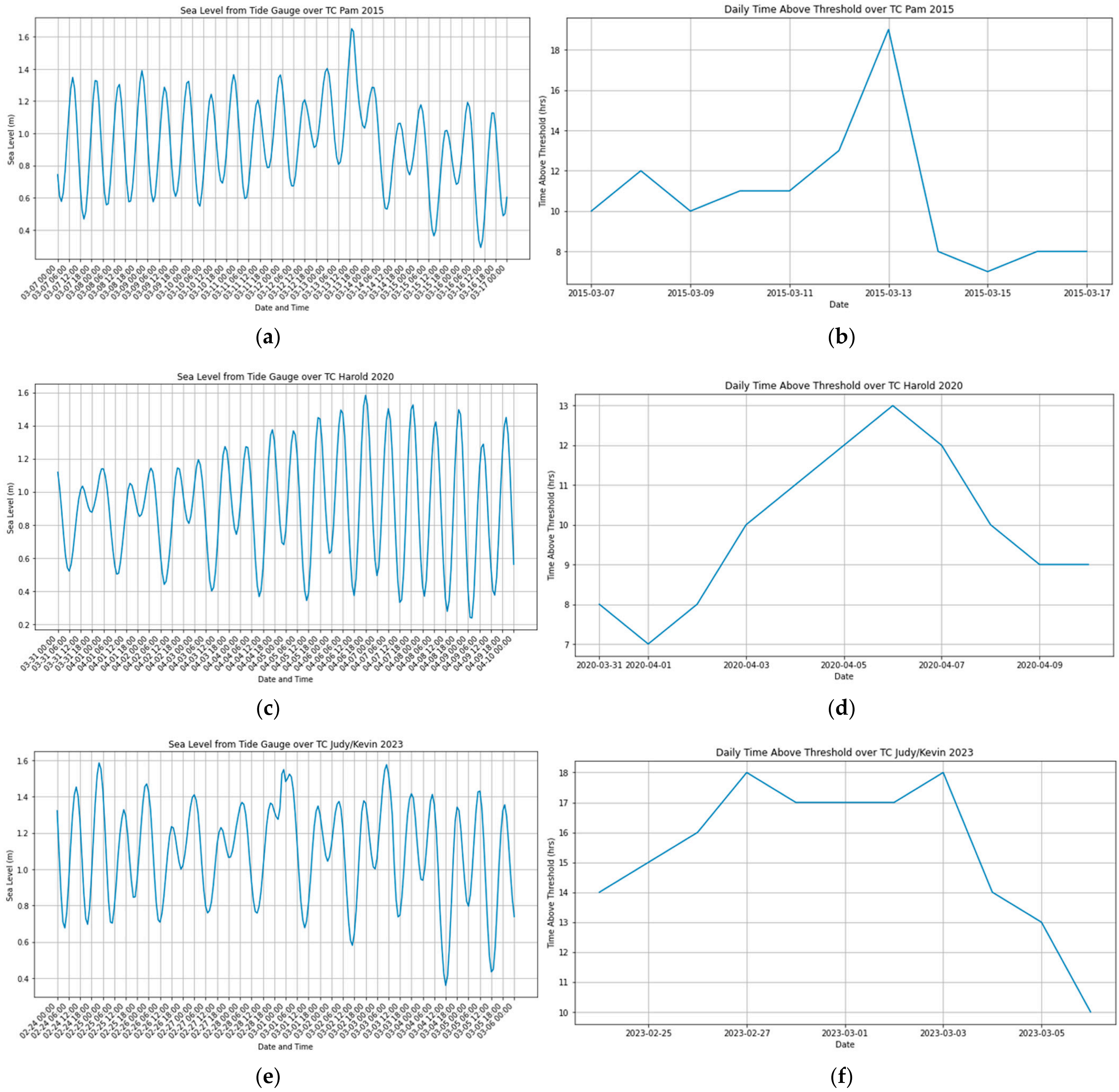

Figure 11. Sea level from Port Vila tide gauge (**left**) and daily Time Above Threshold values (**right**) for three days before and after the five measured event days for TCs Pam (**a**,**b**), Harold (**c**,**d**), and Judy/Kevin (**e**,**f**).

By combining the three surge hazard indicators, CE, SG and TAT, the surge hazard index is created, as shown in Figure 12.

The trends found in CE and SG are seen; however, the magnitude of the values seems to have dropped due to the lower TAT value applied across the country in February compared to the TC case study events. Overall, the highest values are seen in the lagoons and around Eratap, while the southwestern peninsula shows low values due to SG despite having a low-lying elevation. The western main coastline of Port Vila is also relatively low, suggesting reduced surge impacts from TCs to major populations and infrastructure.

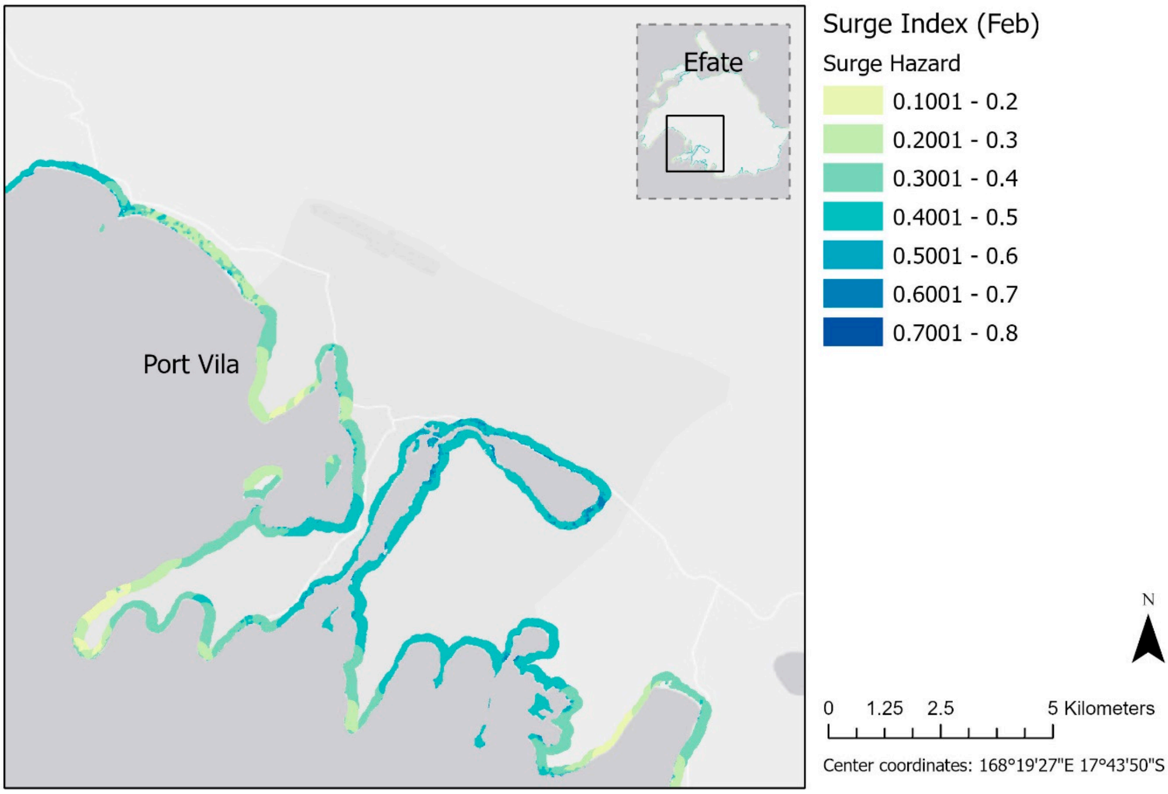

Figure 12. Surge hazard index for February shown over southern Efate Island.

3.3. Exposure and Vulnerability

3.3.1. Population Domain

Figure 13 shows the exposure and vulnerability indicators for the population domain. The exposure in the Population density map (Figure 13a) is highest around Port Vila in Efate Island, as expected, with hotspots along the coast for the islands of Tanna, Malekula and Luganville in Espiritu Santo Island. According to the Distance to Shelter indicator, the most vulnerable regions were in north Espiritu Santo and south Malekula as they were the largest islands with the furthest distances away from buildings used as shelters in TC events. Comparing Distance to Shelter with Population density, there seem to be many shelters, and thus, less vulnerability where major population hubs are. The Economic Stability indicator derived from income source data show high vulnerability over most of the country except for Port Vila and some surrounding Council Areas in Efate. This shows how different residents' jobs are in Vanuatu's capital compared to other islands, which rely on subsistence farming and fishing. Finally, in Figure 13d, the product of exposure and vulnerability for the population domain is depicted with relatively similar values throughout the country. Upon further inspection, many areas have values of 0.1–0.3, either from high exposure and low vulnerability, such as Port Vila, or low exposure with high vulnerability. There are some exceptions where very high values are found in some locations along the coasts of Malekula and Pentecost.

While these indicators give great insight into the population and their characteristics, the input data could still be improved upon. One limitation is the use of income source data as a proxy for a region's financial situation. It assumes people working a job paid wages are less vulnerable than those who receive their income from other methods, such as through the trading of goods or farming. Ideally, a future census could assess expendable income or another indicator of their capacity to persevere through multiple days of disruption to work and repair damages. Additionally, the DtS indicator could be improved with extended information on what people living far away from identified shelters do. This could reveal whether shelter points are missing from the dataset or confirm that they had to brace for

TC landfall in less-than-ideal structures. While this study has tried to select effective and relevant indicators for exposure and vulnerability, with different input data, the pattern shows that the highest risk could change.

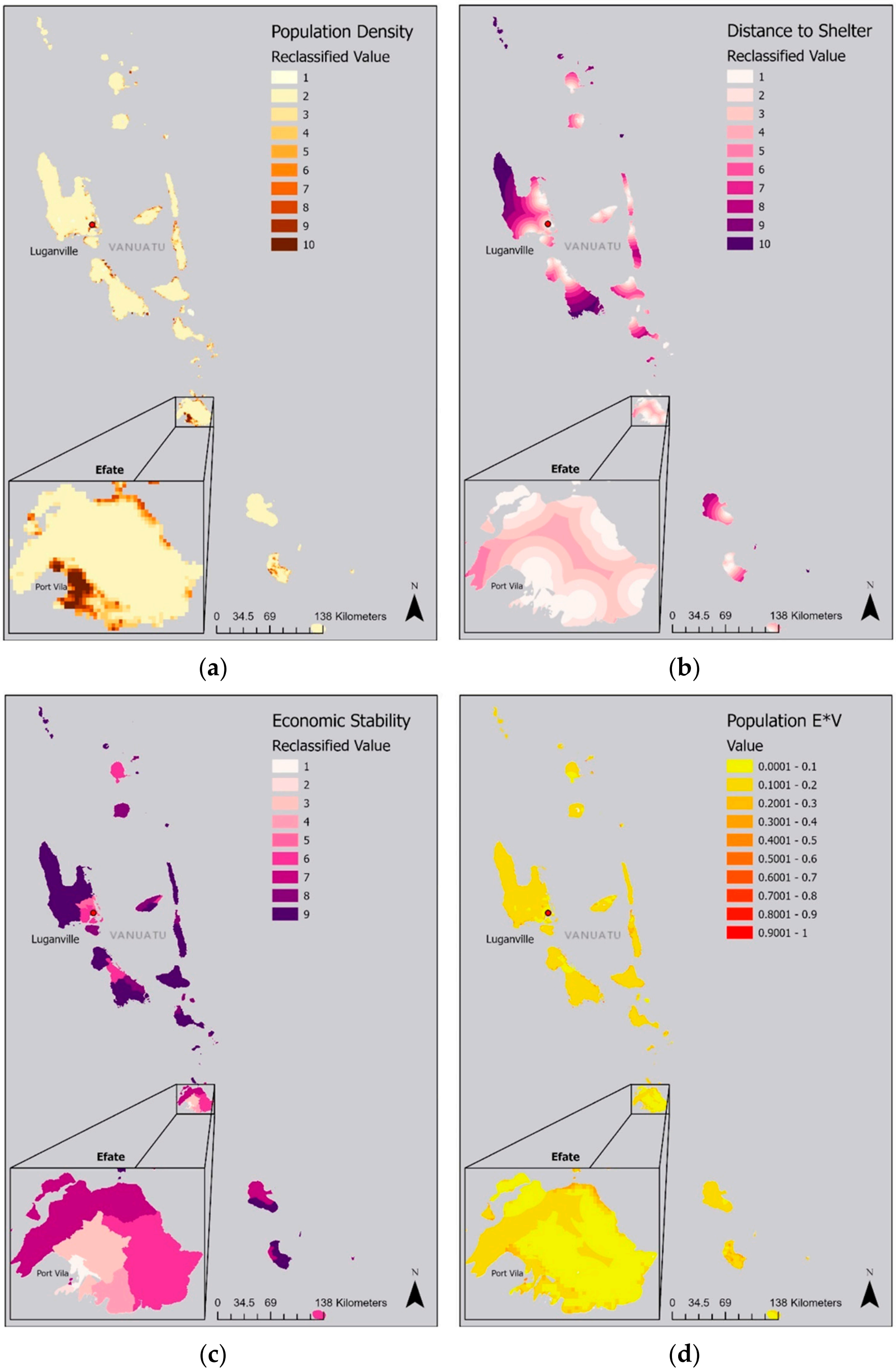

Figure 13. Population density (**a**), Distance to Shelter (**b**), Economic Stability (**c**), and Population Exposure multiplied by vulnerability (**d**). Values are shown over all of Vanuatu with a close-up of the extent of Efate Island. Vulnerability indicators are equally weighted into one vulnerability index before multiplication.

3.3.2. Population Domain

Figure 14 shows the exposure and vulnerability of housing in Vanuatu.

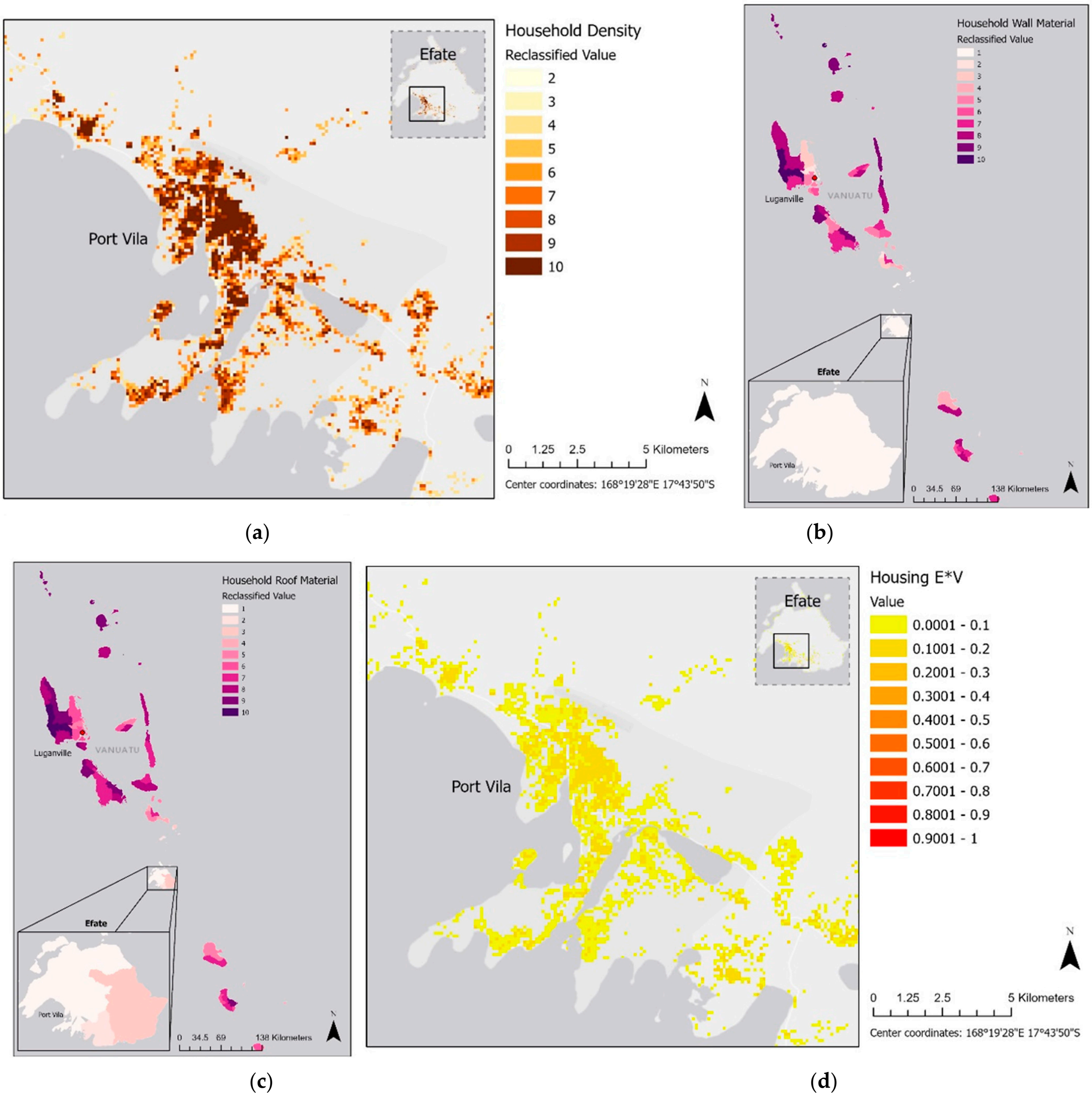

Figure 14. Household Density (**a**), Household Wall Material (**b**), Household Roof Material (**c**), and Housing Exposure multiplied by vulnerability (**d**). Vulnerability indicators are equally weighted into one vulnerability index before multiplication.

Unlike population data, Household Density came in the form of raster data only for areas where houses existed. As a result, there are only data where one or more houses are present. Household Density in the top left shows the highest exposure in Port Vila, as expected, in the capital city. Outside the figure's extent, housing is seen scattered across the country in a similar distribution to Population Density. The vulnerability of housing is quantified by the two indicators of Household Roof Material and Household Wall Material. The material data show Efate Island to have low proportions of their houses built with less sturdy materials, while islands coloured in dark purple have the majority of their houses built from materials such as straw and palm, which are likely to be destroyed in a TC event. The product of exposure and vulnerability for the housing domain can be seen in Figure 14d, showing low values of 0–0.3 around Port Vila due to extremely low vulnerability in comparison to the rest of the country. At hotspots of Household Density across other islands, however, values reach as high as 0.8–0.9 as vulnerability is generally high outside of Efate. The high-resolution but scattered data for housing makes it difficult to ascertain trends at a glance but retains all information from inputs. When analysing risk to housing, data will be summarised into Council Areas for discussion.

3.3.3. Road Domain

Figure 15 shows the exposure and vulnerability of the road domain.

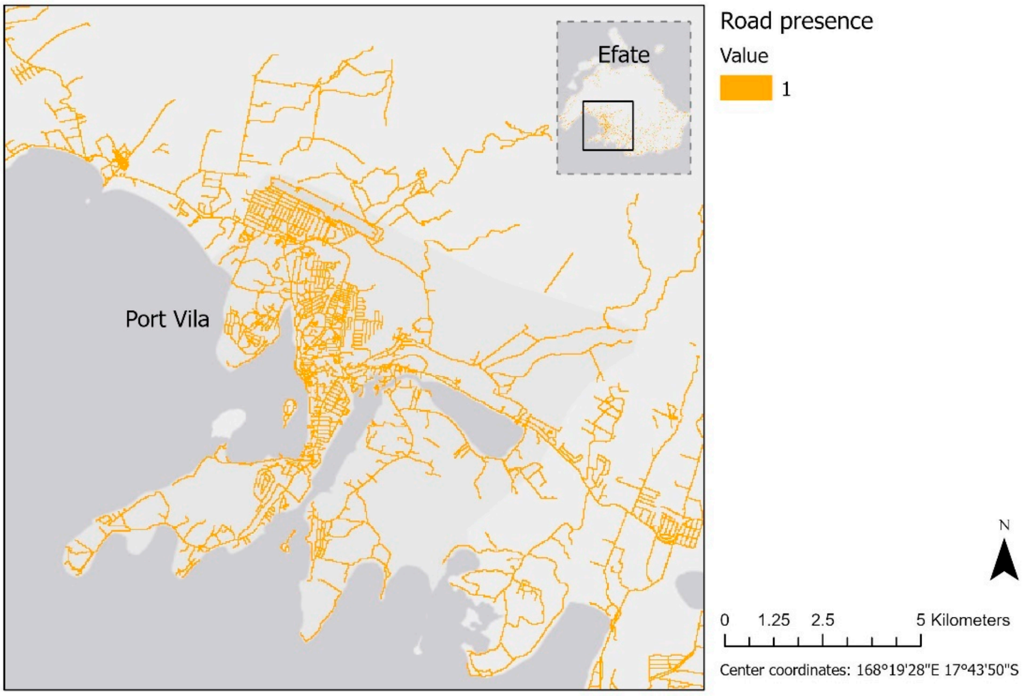

(**a**)

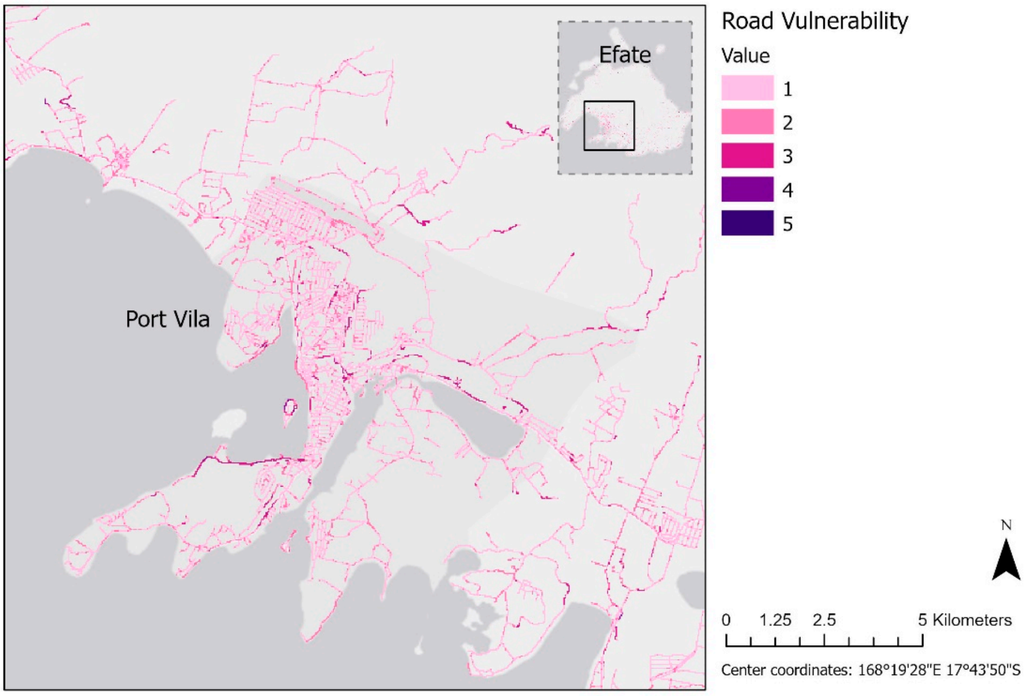

(**b**)

Figure 15. Road exposure is shown by road presence (**a**), and road vulnerability (**b**) is quantified by 5 values relative to the number of vulnerable road conditions that the location satisfies. Results are shown over southern Efate Island.

Exposure is taken as the presence of the road and given a value of one. Although it would have been ideal to differentiate amounts of exposure where there were roads based on road type data (primary roads, secondary roads, trails, etc.), the road data from OpenStreeMap was not complete enough nor verified to be used. Alternatively, statistics such as the amount of traffic each road holds would differentiate the value of different roads, but these data were also not available.

For vulnerability, roads were assessed based on the physical properties of the road's locations, such as the slope. While it is difficult to discern patterns in vulnerability at a glance, they are usually found near the coast or waterways, as can be seen for one road at the southern end of Port Vila along the coastline. Again, not enough road data, such as road surface, were available to indicate how affected the roads would be by water-based hazards, such as surges and floods. A road vulnerability index methodology was instead created using knowledge from the Vanuatu Climate Resilient Road Standards Project, which could easily be replicated in other regions lacking further information from road data.

3.4. Risk Assessment

3.4.1. Flood Risk

Figure 16 shows the flood risk to populations for February as well as the TC case studies.

For each scenario, Efate has higher risk values that are found on the northern coastline, as well as a portion of the coast north of Port Vila. The influence of differing AR values from the hazard index can be seen by consistently higher values from 0.1 and above for northern islands in the case of TC Harold. The TCs Judy and Kevin show an increase in risk values for Efate and more southern islands. In each case, the mountainous northern end of Sanma province, northwest of Luganville, shows consistently higher risk values than other islands. This is likely due to high values from the flood hazard index. The highest risk values shown in red are scarce but exist in particularly coastal regions where there is an overlap of considerable population and high vulnerability. In general, the most populated regions, such as the cities of Port Vila and Luganville, show some of the lowest levels of vulnerability throughout the country, resulting in much lower risk values.

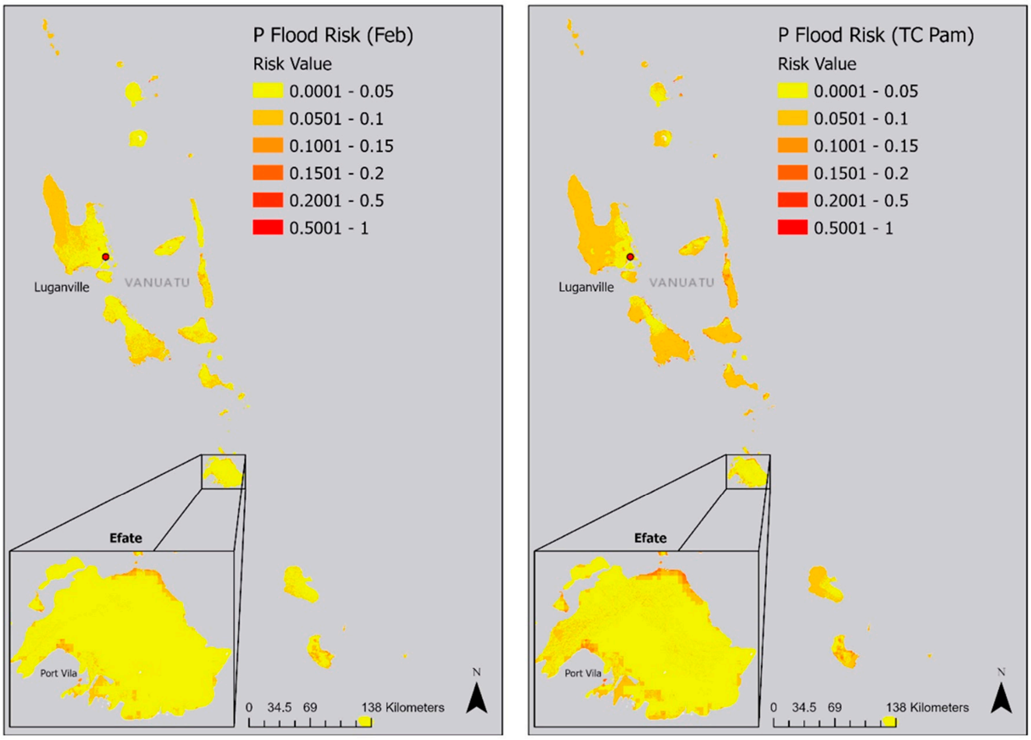

(**a**) (**b**)

Figure 16. *Cont.*

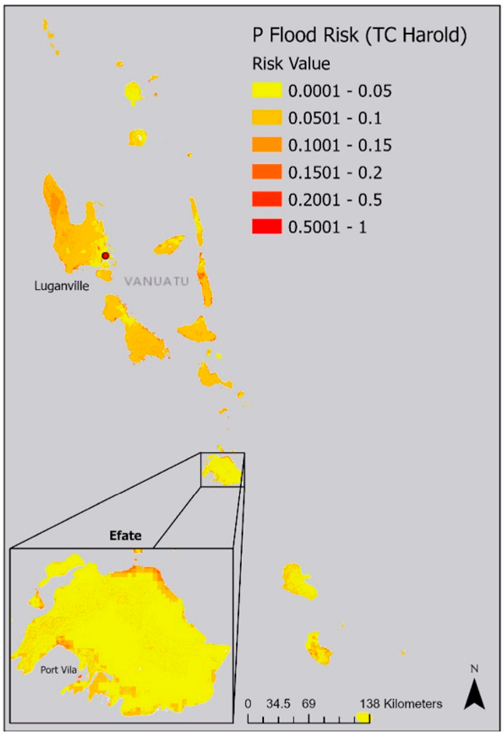

(**c**)

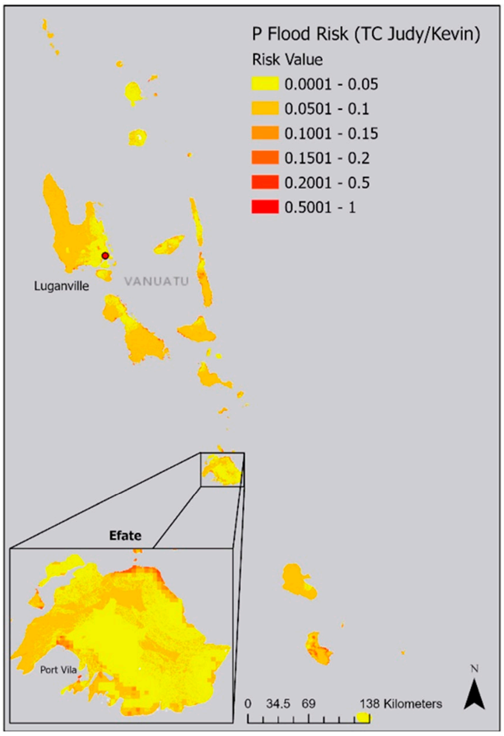

(**d**)

Figure 16. Population flood risk maps for February (**a**), TC Pam (**b**), TC Harold (**c**) and TCs Judy/Kevin (**d**).

While the final risk maps combine trends from all the input indicators, when comparing population flood risk maps of February to historical TC events, where we know they have caused massive devastation and disruption to the country, the risk values seem to be underestimated. This suggests that the weighting of either the hazard or the dynamic AR indicator, in particular, should be emphasised. With the current method, the difference in AR values between scenarios is diluted in the hazard index calculation where it is equally weighted with TWI and impermeability, as well as diluted through multiplication with exposure and vulnerability indices. We expect future validation to confirm this underestimation and prompt adjustments to the methodology.

In the following results, risk values have been summarised to a Council Area resolution for visualisation and to more easily identify trends. Only the February scenario is shown to reduce the repetition of maps, as the case study TC results show the same trends but with an increased relative risk matching the pattern of AR specific to the event.

Figure 17 shows the Council Area mean risk values for the population, housing and road TC flood risks.

While the results were calculated to a high resolution, the values were summarised to the Council Area to allow for a comparison of results at the country zoom level. Figure 17a shows the summarised population flood risk for February, as shown previously in Figure 16. Comparing the domains of populations, households and roads, households show higher risk values, particularly in the northern provinces, while the population risk is moderate-to-low across the country. In general, risk in all domains is relatively low in Efate Island. As the mean value of all cells is taken for each Council Area, population risk values are seen to be lower as the exposure data cover the whole country, whereas households and roads have many gaps. This led to more cells with low exposure values for the population, lowering the overall mean risk.

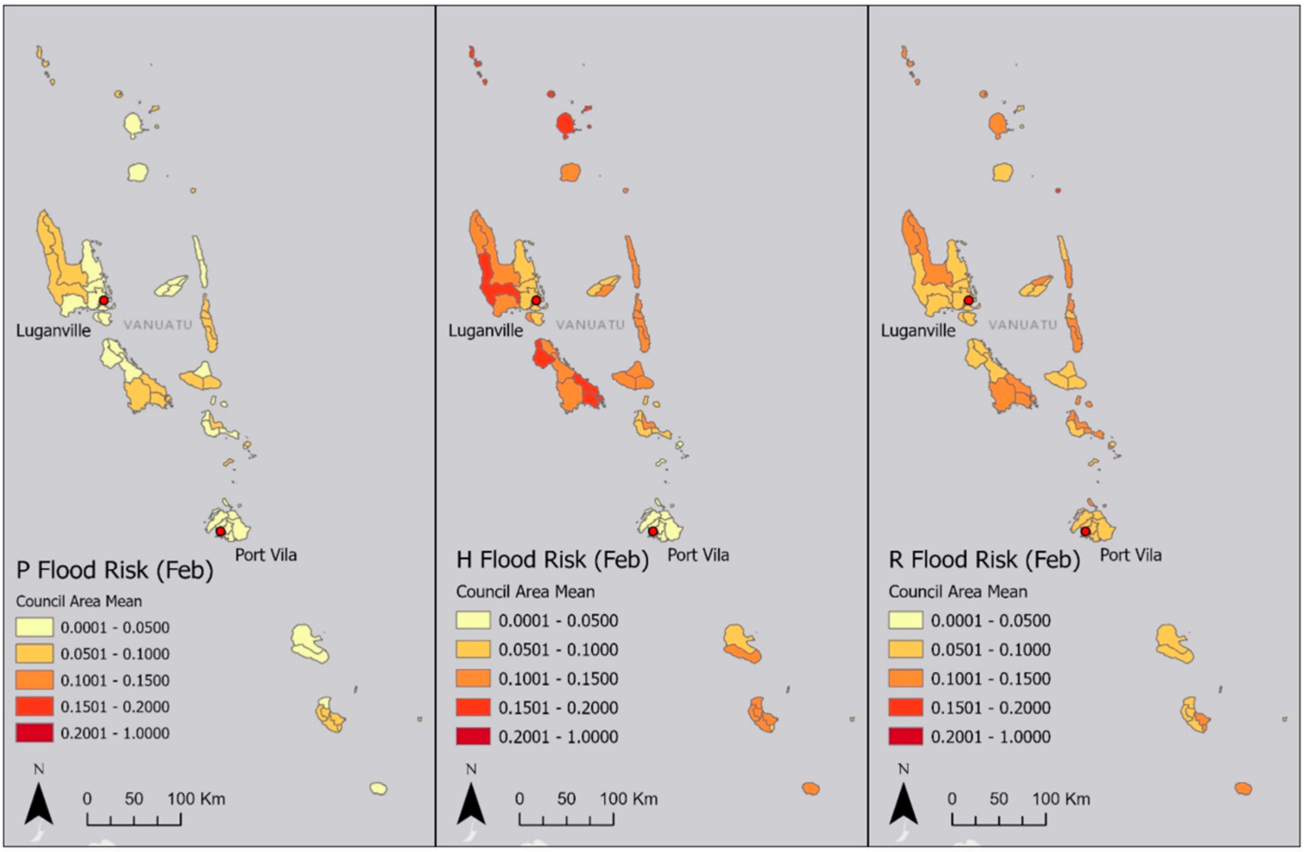

(**a**) (**b**) (**c**)

Figure 17. February flood risk summarised by Council Area for population (**a**), housing (**b**) and road domains (**c**).

Another insight is that the highest exposure but lowest vulnerability regions, such as Efate, particularly in the housing domain, result in much lower risk. While, mathematically, there is no error in the method, it brings up the question of whether the lowest vulnerability based on the chosen indicators is effective in reducing risk in reality. In other words, does Efate's highest proportion of sturdier households dramatically reduce the impacts of TCs. Historical reports suggest that while they may be sturdier, in the event of a severe TC, they are by no means invulnerable to damage and, in most cases, are more expensive to repair, resulting in greater monetary loss. This reveals the need for vulnerability indicators that inform thresholds of whether assets were damaged or not in case study events. One such dataset could be mapped insurance claims; however, these types of data are seldom available in the public domain.

3.4.2. Surge Risk

For surge risk to populations, housing, and roads shown in Figure 18, one can see a very similar pattern to flooding when results are summarised by the Council Area resolution. Risk is generally low in Efate, with roads showing higher values of 0.05–0.15. Compared to the flood risk, the regions of Penama and Tafea provinces reach higher risk values, shown by a darker red.

Figure 18 shows the Council Area mean risk values for population, housing and road TC surge risk. Although surge risk values overall seem to be higher than flood risk, it should be noted that the actual area of surge risk is quite low, only along the coast. TC case study maps were not shown for surge risk as they showed the same trends but with a flat hazard and, hence, risk increase across the country based on each TC event's average TAT value.

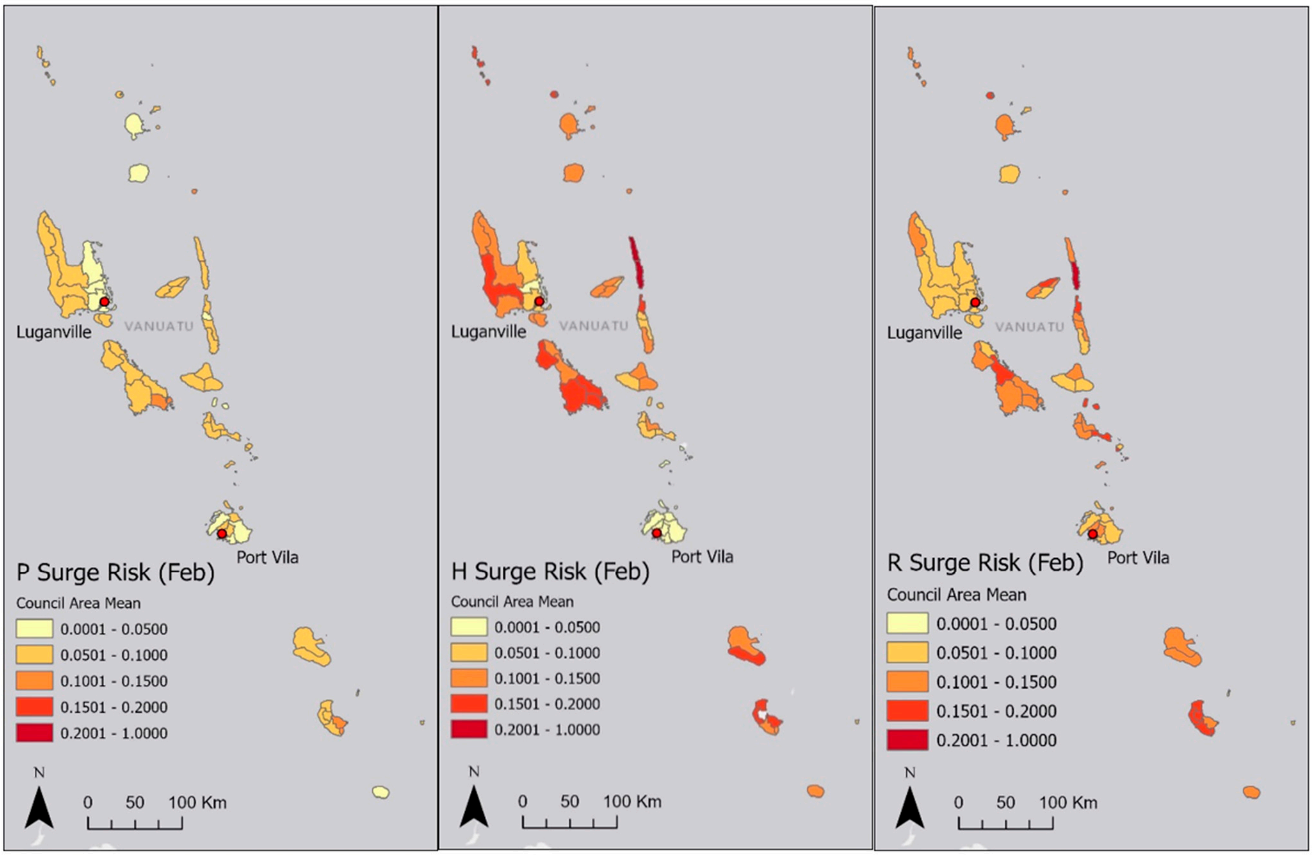

(**a**) (**b**) (**c**)

Figure 18. February surge risk summarised by Council Areas for population (**a**), housing (**b**) and road domains (**c**).

3.5. Further Discussion

The Results and Discussion above have shown how the developed methodology used remote sensing data to indicate TC hazards of flooding and storm surge and how it was applied alongside exposure and vulnerability data for multiple domains to estimate risk. One key missing assessment is the inclusion of wind hazards. This was excluded from the methodology as it was determined that wind hazard is too closely entangled within the TC characteristics of the TC track (location), intensity and wind direction. Removing this information left the possible indicator of surface roughness to determine a location's tendency to allow for high wind speeds; however, compared to indicators such as TWI or CE, surface roughness does not prohibit flooding or storm surge occurrence at a location to the same degree. Thus, winds were excluded from this hazard susceptibility index and risk assessment for Vanuatu; however, we did not understate the impact of wind damage, particularly for Vanuatu and other Pacific Island countries. The inclusion of wind will be a direction of future research.

A limitation of most risk assessments, which are tailored to specific domains or sectors, is that they cannot address every asset at risk. In this study, populations, housing and roads were assessed, and regions of higher and lower risk were identified. A region found with low-risk values for these three domains may be due to the low presence of assessed assets in this location, but in reality, may hold valuable assets such as cropland, critical infrastructure, office buildings or ports. The results shown in this study have mainly been used to identify trends throughout the country and in the main island of Efate. The usefulness of these high-resolution risk maps can only be fully understood when given to local residents who are able to confirm their accuracy or identify gaps.

A benefit of the designed hazard index, along with lower data requirements, is that the hazard describes the susceptibility of the location to flooding and storm surges, even from non-TC events. Any other systems, such as non-cyclonic storms that bring extensive rainfall or winds that push water inland, can have their hazard assessed through this method. While it could be argued that this makes this risk assessment less of a TC-specific risk assessment, it can be adapted to inform decision makers for events no matter where, when, or how strong.

This study contributes to the literature on TC risk assessment by proposing an alternative method of defining hazards and possibly changing how risk assessments can be utilised by decision makers. Although it may seem counterintuitive, removing the probability component of the hazard allows the accompaniment of TC information to be chosen depending on the use case. For example, the risk assessment put forward in this study assessing hazard susceptibility could be accompanied by seasonal TC forecasts [36], sub-seasonal multi-week forecasts [37], or tracks of an incoming TC, which have been improving in recent years. Alternatively, future probabilistic risk information could be inferred by pairing conventional TC hazard model data when they are published or made available.

By setting up the framework in this way, the risk assessment identifies what characteristics of the location make it most susceptible to TC impacts. This shift in focus away from where and how strong TCs may be statistically, instead lends itself to look at what can be changed and improved to increase resilience and reduce the region's vulnerability to TCs.

4. Conclusions

This study evaluated TC risk in Vanuatu, addressing constraints of limited hazard model data in Pacific Island countries. The TC hazard index was modified from earlier studies in Australia to use high-resolution remote sensing data to create proxies for flood and surge hazards. This led to the decision to omit some TC characteristics from the risk assessment, such as predictions of the TC's track, intensity, direction, and duration, and instead focus on quantifying the potential hazard that could occur based on the physical properties of each location; in other words, focusing on hazard susceptibility. With the inclusion of rainfall and tide indicators in each hazard index, this method allowed for the differentiation of rainfall and tide at different time periods. The month of February was assessed using climatologies of accumulated rainfall and Time Above Threshold tide data, compared against the values measured during the following major TC events: TC Pam, TC Harold and TCs Judy and Kevin. As a result, the developed TC risk assessment methodology could be used to inform general future risk, as well as to assess historical events. The risk to the domains of population, housing, and roads were separately assessed. At the fine scale, the results show intersections of high hazard, exposure, and vulnerability scattered across the country; however, maps with values summarised to the Council Area were used to identify trends. These maps show relatively low flood and surge risks over Vanuatu's most populated island of Efate, with higher average risks in the Sanma, Malekula, Tafea and Penama provinces. The comparison of risk in February to TC events with evidence of major impact and disruption to the country suggests the underestimation of the dynamic hazard indicators. Future research will be focused on the comparison of estimated risks against reported impacts in historical TC events, which will allow for the currently developed concept methodology to be evaluated and improved upon.

Author Contributions: Conceptualisation, C.D. and Y.K.; methodology, C.D. and Y.K.; software, C.D.; validation, C.D.; formal analysis, C.D.; investigation, C.D.; resources, Y.K.; data curation, C.D.; writing—original draft preparation, C.D.; writing—review and editing, C.D., Y.K., C.S. and S.C.; visualisation, C.D.; supervision, Y.K., C.S. and S.C.; project administration, Y.K.; funding acquisition, Y.K. All authors have read and agreed to the published version of the manuscript.

Funding: This research has been supported by the Green Climate Fund (GCF) and the Secretariat of the Pacific Regional Environment Programme (SPREP) through the Climate Information Services for Resilient Development in Vanuatu (Van CISRDP) project.

Data Availability Statement: The data presented in this study are available on request from the corresponding author.

Acknowledgments: Authors express sincere gratitude to colleagues from the Climate Risk and Early Warning Systems (CREWS) team at the Australian Bureau of Meteorology and RMIT University for their helpful advice and guidance.

Conflicts of Interest: The authors declare no conflicts of interest.

References

1. World Meteorological Organisation. Tropical Cyclones. Available online: https://wmo.int/topics/tropical-cyclone (accessed on 12 April 2024).
2. Mendelsohn, R.; Emanuel, K.; Chonabayashi, S.; Bakkensen, L. The impact of climate change on global tropical cyclone damage. *Nat. Clim. Chang.* **2012**, *2*, 205–209. [CrossRef]
3. Knutson, T.; Camargo, S.J.; Chan, J.C.L.; Emanuel, K.; Ho, C.-H.; Kossin, J.; Mohapatra, M.; Satoh, M.; Sugi, M.; Walsh, K.; et al. Tropical Cyclones and Climate Change Assessment: Part II: Projected Response to Anthropogenic Warming. *Bull. Am. Meteorol. Soc.* **2020**, *101*, E303–E322. [CrossRef]
4. Deng, Z.; Wang, Z.; Wu, X.; Lai, C.; Zeng, Z. Strengthened tropical cyclones and higher flood risk under compound effect of climate change and urbanization across China's Greater Bay Area. *Urban Clim.* **2022**, *44*, 101224. [CrossRef]
5. Scawthorn, C.; Schneider, P.J.; Schauer, B.A. Natural hazards—The multihazard approach. *Nat. Hazards Rev.* **2006**, *7*, 39. [CrossRef]
6. Burston, J.M.; Taylor, D.; Dent, J.; Churchill, J. Australia-wide tropical cyclone multi-hazard risk assessment. In Proceedings of the Coasts and Ports 2017, Cairns, Australia, 21–23 June 2017; pp. 185–191.
7. Sahoo, B.; Bhaskaran, P.K. Multi-hazard risk assessment of coastal vulnerability from tropical cyclones—A GIS based approach for the Odisha coast. *J. Environ. Manag.* **2018**, *206*, 1166–1178. [CrossRef]
8. Eberenz, S.; Lüthi, S.; Bresch, D.N. Regional tropical cyclone impact functions for globally consistent risk assessments. *Nat. Hazards Earth Syst. Sci.* **2021**, *21*, 393–415. [CrossRef]
9. National Research Council. Hazard and Risk Assessment. In *A Safer Future: Reducing Impacts Natural Disasters*; National Research Council: Washington, DC, USA, 1991; Volume 2, pp. 13–16.
10. Wang, C.; Zhang, H.; Ellingwood, B.R.; Guo, Y.; Mahmoud, H.; Li, Q. Assessing post-hazard damage costs to a community's residential buildings exposed to tropical cyclones. *Struct. Infrastruct. Eng.* **2020**, *17*, 443–453. [CrossRef]
11. Pant, R.; Thacker, S.; Hall, J.W.; Alderson, D.; Barr, S. Critical infrastructure impact assessment due to flood exposure. *J. Flood Risk Manag.* **2018**, *11*, 22–33. [CrossRef]
12. Do, C.; Saunders, G.E.; Kuleshov, Y. Assessment of tropical cyclone risk to coral reefs: Case study for Australia. *Remote Sens.* **2022**, *14*, 6150. [CrossRef]
13. Ivčević, A.; Mazurek, H.; Siame, L.; Moussa, A.B.; Bellier, O. Indicators in risk management: Are they a user-friendly interface between natural hazards and societal responses? Challenges and opportunities after UN Sendai conference in 2015. *Int. J. Disaster Risk Reduct.* **2019**, *41*, 101301. [CrossRef]
14. Rumpf, J.; Weindl, H.; Höppe, P.; Rauch, E.; Schmidt, V. Tropical cyclone hazard assessment using model-based track simulation. *Nat. Hazards* **2009**, *48*, 383–398. [CrossRef]
15. Cardona, O.-D.; Ordaz, M.G.; Mora, M.G.; Salgado-Gálvez, M.A.; Bernal, G.A.; Zuloaga-Romero, D.; Marulanda Fraume, M.C.; Yamín, L.; González, D. Global risk assessment: A fully probabilistic seismic and tropical cyclone wind risk assessment. *Int. J. Disaster Risk Reduct.* **2014**, *10*, 461–476. [CrossRef]
16. Peduzzi, P.; Dao, H.; Herold, C.; Mouton, F. Assessing global exposure and vulnerability towards natural hazards: The Disaster Risk Index. *Nat. Hazards Earth Syst. Sci.* **2009**, *9*, 1149–1159. [CrossRef]
17. Ward, P.J.; Blauhut, V.; Bloemendaal, N.; Daniell, J.E.; de Ruiter, M.C.; Duncan, M.J.; Emberson, R.; Jenkins, S.F.; Kirschbaum, D.; Kunz, M. Natural hazard risk assessments at the global scale. *Nat. Hazards Earth Syst. Sci.* **2020**, *20*, 1069–1096. [CrossRef]
18. Doocy, S.; Dick, A.; Daniels, A.; Kirsch, T.D. The human impact of tropical cyclones: A historical review of events 1980–2009 and systematic literature review. *PLoS Curr.* **2013**, *5*. [CrossRef] [PubMed]
19. Deo, A.; Chand, S.S.; McIntosh, R.D.; Prakash, B.; Holbrook, N.J.; Magee, A.; Haruhiru, A.; Malsale, P. Severe tropical cyclones over southwest Pacific Islands: Economic impacts and implications for disaster risk management. *Clim. Chang.* **2022**, *172*, 38. [CrossRef]
20. Ahmed, I. An Assessment-Based Toolkit for Management of Urban Disasters. In *An Interdisciplinary Approach for Disaster Resilience and Sustainability*; Springer: Singapore, 2020; pp. 497–519. [CrossRef]
21. Heintze, H.-J.; Kirch, L.; Küppers, B.; Mann, H.; Mischo, F.; Mucke, P.; Pazdzierny, T.; Prütz, R.; Radtke, K.; Strube, F. *World Risk Report 2018*; Bündnis Entwicklung Hilft: Berlin, Germany, 2018.
22. Rey, T.; Le De, L.; Leone, F.; Gilbert, D. An integrative approach to understand vulnerability and resilience post-disaster: The 2015 cyclone Pam in urban Vanuatu as case study. *Disaster Prev. Manag. Int. J.* **2017**, *26*, 259–275. [CrossRef]
23. Nalau, J.; Handmer, J.; Dalesa, M. The role and capacity of government in a climate crisis: Cyclone Pam in Vanuatu. In *Climate Change Adaptation in Pacific Countries*; Springer: Cham, Switzerland, 2017; pp. 151–161.

24. Mohanty, S.K.; Chatterjee, R.; Shaw, R. Building resilience of critical infrastructure: A case of impacts of cyclones on the power sector in Odisha. *Climate* **2020**, *8*, 73. [CrossRef]
25. Kaspi, M.; Kuleshov, Y. Flood Hazard Assessment in Australian Tropical Cyclone-Prone Regions. *Climate* **2023**, *11*, 229. [CrossRef]
26. Chipatiso, E. Flood Risk Mapping: Quantifying Topographic Wetness Index to determine Flood Risk Zones for Mutoko District in Zimbabwe. *J. Sens. Netw. Data Commun.* **2023**, *3*, 215–222.
27. Irish, J.L.; Resio, D.T. A hydrodynamics-based surge scale for hurricanes. *Ocean Eng.* **2010**, *37*, 69–81. [CrossRef]
28. Islam, M.R.; Lee, C.-Y.; Mandli, K.T.; Takagi, H. A new tropical cyclone surge index incorporating the effects of coastal geometry, bathymetry and storm information. *Sci. Rep.* **2021**, *11*, 16747. [CrossRef] [PubMed]
29. Gori, A.; Lin, N.; Xi, D. Tropical Cyclone Compound Flood Hazard Assessment: From Investigating Drivers to Quantifying Extreme Water Levels. *Earth's Future* **2020**, *8*. [CrossRef]
30. Hague, B.S.; Murphy, B.F.; Jones, D.A.; Taylor, A.J. Developing impact-based thresholds for coastal inundation from tide gauge observations. *J. South. Hemisph. Earth Syst. Sci.* **2020**, *69*, 252–272. [CrossRef]
31. Do, C.; Kuleshov, Y. Multi-hazard Tropical Cyclone Risk Assessment for Australia. *Remote Sens.* **2023**, *15*, 795. [CrossRef]
32. PACCSAP; SMEC; Government of Vanuatu. The Vanuatu Climate Resilient Road Standards Project. 2014. Available online: https://www.pacificclimatechange.net/sites/default/files/Vanuatu-Climate-Resilient-Road-Standards-brochure.pdf (accessed on 2 November 2023).
33. Crichton, D. UK and global insurance responses to flood hazard. *Water Int.* **2002**, *27*, 119–131. [CrossRef]
34. Schneiderbauer, S.; Ehrlich, D. Risk, hazard and people's vulnerability to natural hazards. In *A Review of Definitions, Concepts and Data*; European Commission Joint Research Centre: Brussels, Belgium, 2004; Volume 21410, p. 40.
35. Rabine, C. *Timing of Tectonic Uplift Rate Change at Araki, Vanuatu, Derived from 230-Th Dating of Fossil Corals*; University of Minnesota: Minneapolis, MN, USA, 2018.
36. Takaya, Y.; Caron, L.-P.; Blake, E.; Bonnardot, F.; Bruneau, N.; Camp, J.; Chan, J.; Gregory, P.; Jones, J.J.; Kang, N. Recent advances in seasonal and multi-annual tropical cyclone forecasting. *Trop. Cyclone Res. Rev.* **2023**, *12*, 182–199. [CrossRef]
37. Schreck, C.J., III; Vitart, F.; Camargo, S.J.; Camp, J.; Darlow, J.; Elsberry, R.; Gottschalck, J.; Gregory, P.; Hansen, K.; Jackson, J. Advances in tropical cyclone prediction on subseasonal time scales during 2019–2022. *Trop. Cyclone Res. Rev.* **2023**, *12*, 136–150. [CrossRef]